



1 **Measurement report: The influence of traffic and new particle**
2 **formation on the size distribution of 1-800 nm particles in Helsinki:**
3 **a street canyon and an urban background station comparison**

4 Magdalena Okuljar¹, Heino Kuuluvainen², Jenni Kontkanen¹, Olga Garmash¹, Miska Olin², Jarkko V. Niemi³,
5 Hilikka Timonen⁴, Juha Kangasluoma¹, Yee Jun Tham¹, Rima Baalbaki¹, Mikko Sipilä¹, Laura Salo²,
6 Henna Lintusaari², Harri Portin³, Kimmo Teinilä⁴, Minna Aurela⁴, Miikka Dal Maso², Topi Rönkkö², Tuukka
7 Petäjä¹ and Pauli Paasonen¹

8 ¹Institute of Atmospheric and Earth System Science / Physics, Faculty of Science, University of Helsinki,
9 FI-00014, Helsinki, Finland

10 ²Aerosol Physics Laboratory, Physics Unit, Tampere University, PO Box 692, FI-33014, Tampere, Finland

11 ³Helsinki Region Environmental Services Authority, PO Box 100, FI-00066, Helsinki, Finland

12 ⁴Atmospheric Composition Research, Finnish Meteorological Institute, PO Box 503, FI-00101, Helsinki, Finland

13 *Correspondence to:* Magdalena Okuljar (magdalena.okuljar@helsinki.fi)

14 **Abstract.** Most of the anthropogenic air pollution sources are located in urban environments. The contribution of these
15 sources to the population of atmospheric particles in the urban environment is poorly known. In this study, we investigated
16 the aerosol particle number concentrations in a diameter range from 1 to 800 nm at a street canyon site and at a background
17 station within 1 km from each other in Helsinki, Finland. We use these number size distribution data together with
18 complementary trace gas data and develop a method to estimate the relative contributions of traffic and atmospheric new
19 particle formation (NPF) to the concentrations of sub-3 nm particles. During the daytime, the particle concentrations were
20 higher at the street canyon site than at the background station in all analyzed modes: sub-3 nm particles, nucleation mode
21 (3-25 nm), Aitken mode (25-100 nm), and accumulation mode (100-800 nm). The population of sub-3 nm and nucleation
22 mode particles was linked to local sources such as traffic, while the accumulation mode particles were more related to
23 non-local sources. Aitken mode particles were dominated by local sources at the street canyon site while at the background
24 station they were mainly influenced by non-local sources. The results of this study support earlier research showing direct
25 emissions of the sub-3 nm particles from traffic. However, by using our new method, we show that during NPF events,
26 traffic contribution to the total sub-3 nm particle concentration can be small and during daytime (6:00-20:00) in spring it
27 does not dominate the sub-3 nm particle population at either of the researched sites. In the future, this method can be
28 applied to estimate the contribution of traffic to particle number concentrations in different urban environments. This
29 knowledge is needed to evaluate the effects of traffic on urban air quality.

30 **1. Introduction**

31 Aerosol particles are both directly emitted to the atmosphere (primary particles) and formed from gaseous precursors
32 (secondary particles) (Kulmala and Kerminen, 2008). Secondary particles can form by new particle formation (NPF) via
33 atmospheric photochemical reactions or nucleate in plumes from local sources (Kerminen et al., 2018; Mylläri et al.,
34 2016). Additionally, particles may form while hot vehicle exhaust is cooled and diluted, which is called delayed primary
35 particulate matter formation (Rönkkö and Timonen, 2019). The urban environment contains a mixture of secondary
36 particles, and primary particles emitted from a variety of industrial processes, traffic, power generation, and natural
37 sources (Seinfeld and Pandis, 2016). Aerosol particles influence the visibility (Hyslop, 2009), the hydrological cycle
38 (Rosenfeld et al., 2008), and radiation balance (Andreae, 2009; Ramanathan and Feng, 2009). Furthermore, particles can



39 harm human health, impacting respiratory and cardiovascular systems (André, 2014). Urban air pollution also contains
40 magnetite nanoparticles, which accumulate in the brain, and may cause neurodegenerative diseases (Maher et al., 2016).
41 Nanoparticles with diameters below 3 nm may have significant, so far poorly understood, health effects due to their nose-
42 to-brain transport via the olfactory pathway (Tian et al., 2019). Models show that outdoor air pollution causes
43 approximately 400 000 premature deaths in Europe annually (Geels et al., 2015; Im et al., 2018), from which around 2000
44 take place in Finland (Im et al., 2019). These numbers do not include the possible impacts of above mentioned health
45 impacts of nanoparticles.

46 In recent years, instrument development has enabled the detection of aerosol particles with diameters between 1 and 3 nm
47 (Vanhanen et al., 2011), which we here refer to as sub-3 nm particles. This had made it possible to study the very
48 beginning of NPF, which starts with the formation of sub-3 nm particles. NPF events are favored in specific
49 meteorological conditions, for example, high solar radiation and low relative humidity, as well as an abundance of low-
50 volatile gaseous precursors (Hussein et al., 2008; Kerminen et al., 2018; Salma et al., 2011; Wonaschütz et al., 2015).
51 One of the known gaseous precursors, which plays an important role in NPF, is sulfuric acid (SA). SA is an oxidation
52 product of sulfur dioxide (SO₂), which is primarily emitted from anthropogenic processes related to fuel combustion, for
53 example from traffic. Previous studies have shown that SA is also directly (Arnold et al., 2012; Rönkkö et al., 2013) and
54 indirectly via solar radiation (Olin et al., 2020) emitted by traffic. In many locations, SA concentration is one of the critical
55 factors determining whether NPF occurs (Kuang et al., 2008; Ripamonti et al., 2013; Wang et al., 2011).

56 In addition to potential NPF events, traffic is a significant source of the sub-3 nm particles (Hietikko et al., 2018; Rönkkö
57 et al., 2017). The sub-3 nm particles are directly emitted from vehicle exhaust and brake wear (Nosko et al., 2017) or
58 formed in the exhaust plume from the nucleating gaseous components (Rönkkö and Timonen, 2019). On the other hand,
59 the concentrations from the road emissions decrease fast while moving away from a road due to dispersion (Pirjola et al.,
60 2006). Especially, the concentration of the sub-3 nm particles is additionally reduced by condensation and coagulation
61 (Kangasniemi et al., 2019). Rönkkö et al. (2017) showed that the sub-3 nm particles represent 20-54% of the particle
62 population in a 'semiurban' roadside environment in Helsinki. Kontkanen et al. (2017) analyzed the sub-3 nm particle
63 concentrations in different environments and concluded that the sub-3 nm particle concentrations are higher in locations
64 influenced by anthropogenic emissions. Detailed analysis has linked the sub-3 nm particles to traffic activity and traffic
65 emissions at the street canyon in Helsinki (Hietikko et al., 2018). Traffic emissions do not only contain particles but also
66 SA, volatile organic compounds, and trace gases for example carbon dioxide (CO₂) and nitrogen oxides (NO_x), which are
67 commonly used as traffic markers. Generally, the role of traffic in urban air quality and its effects on human health are
68 still not well understood.

69 Previously, particle size distributions have been measured in different urban environments, such as London (Bousiotis et
70 al., 2019; Harrison et al., 2019; Hofman et al., 2016), Stockholm (Mårtensson et al., 2006), Innsbruck (Deventer et al.,
71 2018), Los Angeles (Zhu et al., 2002), Beijing (Zhou et al., 2020), Shanghai (Xiao et al., 2015), and Helsinki (Hussein et
72 al., 2006; Ripamonti et al., 2013). In the Helsinki area, the focus of the research has been either on NPF (Hussein et al.,
73 2008, 2009) or the primary particle emissions (Hietikko et al., 2018; Ripamonti et al., 2013; Rönkkö et al., 2017). These
74 approaches leave an open question about the relative contribution of each source to the particle population. To answer
75 this question, we conducted simultaneous measurements at two close-by stations in the Helsinki area: at the street canyon
76 and at the urban background station. For the first time, particle size distribution in a diameter range from 1 to 800 nm as
77 well as the concentrations of precursor gases were simultaneously measured at two nearby stations in Helsinki. In this

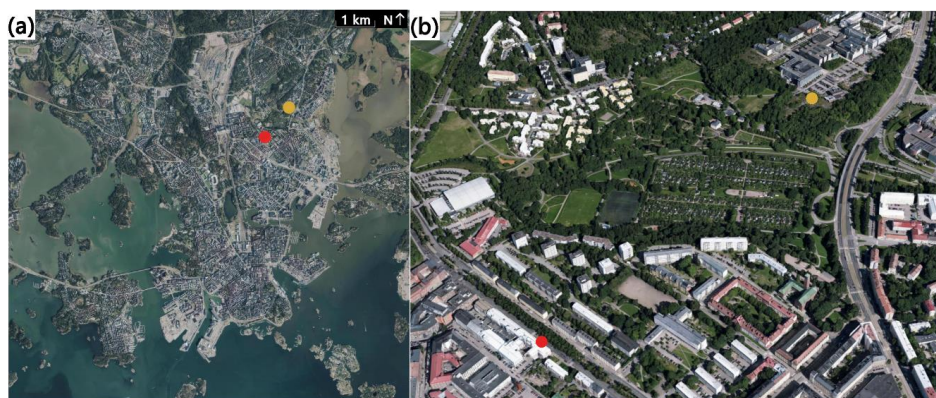


78 article, we present the results of these measurements and compare the particle size distributions and their variation at
79 these two stations. Specifically, we develop and apply a new method to determine the relative contributions of NPF and
80 traffic to the sub-3 nm particle population in different urban environments.

81 2. Methods

82 2.1. Measurement stations

83 We performed measurements at two different stations in Helsinki, Finland, during April-June 2018. The first one is
84 Helsinki Region Environmental Services (HSY) air quality station, which is placed in a street canyon (Mäkelänkatu street,
85 approximately 28 000 vehicles per workday) and represents a busy street environment (Kuuluvainen et al., 2018). The
86 second one, the Station for Measuring Ecosystem-Atmosphere Relations (SMEAR III), is located within 900 m north-east
87 of HSY site, and it is classified as an urban background station (Fig. 1) (Järvi et al., 2009). The sites are separated by
88 buildings, a botanic garden, and a small deciduous forest. The SMEAR III is located on a hill, approximately 12 m above
89 the nearest busy road (Hämeentie street). The SMEAR III is separated from Hämeentie by a 150 m band of a deciduous
90 forest. Apart from the forest, in the SMEAR III surrounding are also buildings, parking lots, and small vegetation (Järvi
91 et al., 2009). In this article, the two measurement stations are called ‘street canyon’ and ‘background’, respectively.



92 Figure 1. Aerial photography (a) and 3d model (b) of stations: street canyon (red) and background (yellow). The
93 photograph and the model were provided by The City of Helsinki map service (CC BY 4.0).

94 2.2. Measurement period and comparison of data from sites

95 We measured particle number size distribution, trace gas and SA concentrations at both stations during the period 27 April
96 2018 – 5 June 2018. An overview of instruments used during this campaign is presented in Table 1 indicating the total
97 running time at each station. The detailed working time for each instrument is shown in Table A1. Most of the analysis
98 was conducted separately for workdays and days free of work, i.e. weekends and holidays (1 May 2018 and 10 May
99 2018), which are for simplicity just referred to as ‘weekends’ in this article. When comparing particle concentrations from
100 two stations, we analyze times when all the instruments measuring particles were performing at each site. This resulted
101 in 120 and 101 hours of measured particle concentration during weekends and workdays, respectively, at the street canyon
102 site. At the background station, it resulted in 217 hours of observed particle concentration during weekends and 398 hours
103 during workdays. In addition, we present separately a few case studies, where the overlapping data obtained



104 simultaneously from two stations are analyzed in more detail. Oppositely to the analysis of particle concentrations,
105 sulfuric acid (SA) concentration was studied only for the overlapping period of measurements at two stations resulting in
106 167 and 329 hours measured during weekends and workdays, respectively. Condensation sink (CS) was studied from the
107 same time frame as SA.

108 **2.3. Particle size distribution measurement**

109 A wide range of particle size distribution was obtained by combining several instruments: a Particle Size Magnifier (PSM)
110 (Vanhanen et al., 2011), an Ultrafine Condensation Particle Counter (UCPC), and a Condensation Particle Counter (CPC)
111 (Kangasluoma and Attoui, 2019) as well as a Differential Mobility Particle Sizer (DMPS) (Wiedensohler et al., 2012).
112 The measured size ranges and working hours of these instruments are presented in Table 1.

113 The PSM technique contains a pre-conditioner, that activates the smallest particles and grows them up to 90 nm, and a
114 CPC (Vanhanen et al., 2011). The minimum size of activated particles depends on the diethylene glycol supersaturation
115 in the pre-conditioner (Lehtipalo et al., 2014). Altering the supersaturation condition allows varying the minimum size of
116 activated and measured particles between 1 and 3 nm. The PSM can be used to measure particle concentrations in three
117 different modes: fixed, step, and scanning. In the fixed mode, supersaturation and the minimum size of the measured
118 particles are constant. Data obtained by measuring in the fixed mode have a high temporal resolution (1 s), and therefore
119 it is mainly used in a very rapidly changing environment such as a busy street. In the step mode, supersaturation and the
120 lowest size of measured particles oscillate between three set values. This allows analyzing particle size distribution in the
121 range from 1 to 3 nm. On the other hand, data obtained from step mode measurements have a lower temporal resolution
122 (3 min). Adjusting the time of every supersaturation measurement allows minimizing the uncertainties related to the rapid
123 changes in the analyzed environment. In the scanning mode, supersaturation gradually changes between two set values.
124 The scanning mode enables choosing the size bins when inverting the raw data to a size distribution. However, the
125 temporal resolution of scanning mode is the lowest of all the modes (4 min). In the scanning mode, we assume that particle
126 concentration stays constant during each scan, thus this mode cannot be used in a rapidly changing environment. In this
127 study, PSM was operated in fixed and step modes. At both stations, PSMs working in the fixed mode measured
128 concentrations of particles with sizes larger than 1.2 nm.

129 Condensation particle counters enlarge particles by condensation of supersaturated condensable vapors. Once particles
130 reach a size sufficient for optical detection, they are counted by the optical particle counter. In this study, we use two
131 models of butanol-based CPCs, from which one measures particle concentration of particles with sizes larger than 3 nm,
132 while the other one counts particles with sizes larger than 7 nm. For simplicity, we call them UCPC and CPC, respectively.

133 Differential mobility particle sizer (DMPS) consists of a differential mobility analyzer (DMA) and a CPC. The DMA
134 classifies charged particles according to their mobility in an electric field. By incrementally stepping the voltage applied
135 to the central rod of the DMA, particles of lower mobility can be classified by the DMA and further quantified by the
136 CPC. During an 8 minute cycle, DMPS monitors the size distribution of particles with a diameter between 6 and 800 nm.
137 The size distribution obtained from DMPS measurements was used to study the loss rate of vapors due to condensation
138 on existing particles, i.e. CS (Kulmala et al., 2012). DMPS data from the background station was also utilized to identify
139 NPF events based on the method proposed by Dal Maso et al. (2005).



140 All instruments were corrected for diffusion losses in their inlets except the UCPC measuring at the background station,
141 in which the core sampling technique (Fu et al., 2019) was used.

142 Sub-3 nm particle concentration was determined by subtracting concentration measured by the UCPC from concentrations
143 measured by the PSM working at the fixed mode. The nucleation mode (3-25 nm) was computed by adding concentration
144 measured by DMPS with diameters of 7-25 nm to the difference of concentration measured by CPC and UCPC. Particle
145 concentrations measured by DMPS with diameters of 25-100 nm and 100-800 nm were considered the Aitken and
146 accumulation mode concentrations. The size range for the Aitken mode corresponds to the range of mean particle size in
147 the typical soot mode of vehicle exhaust (Rönkkö and Timonen, 2019). At the street canyon site, gaps in the UCPC data
148 were filled with the concentration of particles larger than 3 nm obtained from the PSM measuring in the step mode. At
149 the background station, UCPC data from 29 May to 4 June were corrected by checking that the ratios of concentrations
150 measured with the PSM and UCPC as well as UCPC and CPC agree in the night-time. All the measured size ranges
151 correspond to the mobility diameter of particles.

152 Table 1. Overview of the main instruments used at the street canyon and background station during the campaign.

Instrument	Description	Working time at street canyon [h]	Working time at background station [h]
PSM (fixed mode)	Concentration of particles larger than 1.2 nm	246	766
PSM (step mode)	Particle size distribution in the range of 1-3 nm	833	-
UCPC	Concentration of particles larger than 3 nm	548	670
CPC	Concentration of particles larger than 7 nm	750	728
DMPS	Particle size distribution in the range of 6-800 nm	840	821
CI-API-TOF	Concentration and chemical identification of vapor molecules and molecular clusters in size range approximately 0.1-1 nm. In this study only sulfuric acid concentration is utilized.	501	776
SO ₂ analyzer	Concentration of SO ₂ on ppb level	452	937
CO ₂ analyzer	Concentration of CO ₂ on ppm level	771	248
NO/NO _x analyzer	Concentration of NO/NO _x on ppm level	937	937

153 2.3.1. Uncertainties of sub-3 nm particles measurement

154 Measuring the concentration of particles smaller than 3 nm contains noteworthy uncertainties mainly due to the effect of
155 chemical composition and charging state of particles on the cutoff size of PSM.

156 Particle detection efficiency in butanol counters (Wlasits et al., 2020) and the PSM techniques depend strongly on the
157 chemical composition of measured clusters. Experiments show that the difference between the cutoff diameter in PSM
158 for particles with different chemical composition can reach up to approximately 1 nm (Jiang et al., 2011; Kangasluoma
159 et al., 2014, 2016). This causes uncertainty of ± 0.5 nm for particles with unknown chemical composition. PSM calibrated
160 with particles with the same chemical composition as measured one would have a negligible offset (Kangasluoma et al.,



161 2015). In the urban environment, the chemical composition of particles is complex and evolving with time, thus this
162 uncertainty cannot be minimized in this research.

163 Uncertainty due to the charging state of particles is mainly affected by the discrepancy between the charging state of
164 measured particles and particles used for the calibration. PSMs were calibrated with negatively charged tungsten oxide
165 clusters by the method presented in Kangasluoma et al. (2015). However, the majority of particles measured in the urban
166 environment are likely electrically neutral (Yao et al., 2018). Since neutral particles are activated at a higher
167 supersaturation than charged particles, we probably underestimate the size of measured particles (Kangasluoma et al.,
168 2016, 2017; Winkler et al., 2008). Experiments indicate a 0.1-0.5 nm increase in the activated diameter of neutral particles
169 in PSM in comparison to the charged ones (Kangasluoma et al., 2016, 2017). When the effect of charge on the measured
170 particle population is unknown, increasing the cutoff diameter in PSM by 0.3 nm will reduce the uncertainty of the state
171 of charge to ± 0.2 nm (Kangasluoma and Kontkanen, 2017).

172 Additionally, meteorological conditions such as humidity can affect the cutoff size of PSM and CPC (Kangasluoma et
173 al., 2013; Tauber et al., 2019).

174 Lastly, the non-ideal efficiency curve, used for determining the cutoff diameter, makes it possible to sample particles
175 smaller than the cutoff size. When the relative contribution of sub-3 nm particles to the total particle population is high,
176 the uncertainties of cutoff diameter or the shape of the efficiency curve can affect the total concentration measured by
177 PSM and CPC (Kangasluoma and Kontkanen, 2017).

178 **2.4. Sulfuric acid measurement**

179 Sulfuric acid (SA) concentration was monitored with a high-resolution chemical ionization atmospheric pressure interface
180 time-of-flight mass spectrometer (CI-API-TOF) with nitrate (NO_3^-) as a reagent ion. CI-API-TOF technique contains a
181 chemical ionization source (CI) and an atmospheric pressure interface (APi) coupled with a time-of-flight mass
182 spectrometer (TOF). Chemical ionization is a soft ionization technique in which the reagent ion reacts with analyzed
183 compounds and charge them. NO_3^- is a reagent ion used for the detection of gaseous SA in ambient air (Eisele and Tanner,
184 1993; Jokinen et al., 2012; Mauldin et al., 1999). NO_3^- or its cluster with nitric acid ($\text{HNO}_3\text{NO}_3^-$) reacts via proton transfer
185 reaction with sulfuric acid creating a cluster detectable by the APi-TOF technique (Jokinen et al., 2012). A detailed
186 description of nitrate-based CI method used as a pre-treatment for APi-TOF technique is presented by Jokinen et al.
187 (2012). The atmospheric pressure interface guides ionized compounds through three stages of lowering sample pressure
188 to the time-of-flight region. A TOF mass spectrometer separates and detects analyzed compounds by their mass-to-charge
189 ratios. A detailed description of the APi-TOF technique is described by Junninen et al. (2010).

190 Due to the uncertainty of the rate of the reaction between gaseous sulfuric acid and the nitrate ion, the CI-API-TOF needs
191 to be calibrated by taking the wall losses of SA inside the instrument and the flow conditions of the ion source into
192 consideration (Kürten et al., 2012; Viggiano et al., 1997). Calibration of CI-API-TOF was done before the campaign,
193 based on the method proposed by Kürten et al. (2012). The SA concentration was calculated from Eq (1) (Jokinen et al.,
194 2012).

195

$$[\text{SA}] = C \cdot \frac{\text{CR}_{97} + \text{CR}_{160}}{\text{CR}_{62} + \text{CR}_{125} + \text{CR}_{188}} \quad (1)$$



196 where [SA] is SA concentration, C is the calibration coefficient and CR_M is a count rate of an ion with a mass M in
197 amu.
198 The SA zero level concentration, determined by measuring filtered air, was subtracted from the measured concentrations.
199 Uncertainties of absolute concentration measured by CI-API-TOF are in the order of 50%, while the uncertainties of
200 relative changes in the concentration are smaller than 10% (Ehn et al., 2014).

201 **2.5. Other instrumentation**

202 Nitric oxide (NO), CO₂, SO₂, and NO_x were additionally measured during this campaign (Table 1). To complement these
203 measurements, we used continuous measurements performed at both stations. These include meteorological parameters,
204 ozone (O₃) concentration, ion size distribution, and black carbon (BC) concentration. All the instruments used are listed
205 in Table A2.

206 **2.6. Estimation of the relative contribution of NPF and traffic to sub-3 nm particles**

207 To estimate the influence of traffic and NPF on the sub-3 nm particle population, we analyzed the correlation between
208 sub-3 nm particles and NO_x concentrations as well as between sub-3 nm particles and SA concentrations. NO_x
209 concentration was used as a traffic marker (Olin et al., 2020) while SA concentration was used as an NPF marker (Sipila
210 et al., 2010). Bivariate fittings (Cantrell, 2008; Williamson, 1968; York, 1966) were conducted on the common logarithms
211 of sub-3 nm particles and SA when NO_x concentration was low to estimate sub-3 nm particles concentration originating
212 from NPF. Correlation between common logarithms of sub-3 nm particles and NO_x, when SA concentration was low,
213 was used to estimate sub-3 nm particle concentration originating from traffic. Equations used for calculating sub-3 nm
214 particles emitted by traffic and NPF as well as their relative contributions to the particle population are presented in the
215 Appendix (Eq. A1-A6).

216 **3. Results and Discussion**

217 **3.1. NPF event classification**

218 The results of the NPF event classification at the background station for the studied period is shown in Table 2. The
219 examples of an event, non-event, and undefined class are shown in Fig. S1. The overall frequency of NPF event days was
220 12.5%; 21% of weekends and 8% of workdays were classified as events. Due to nucleation mode particles originating
221 from local sources, the majority of days were classified as undefined.

222 Table 2. NPF event classification at the background station for the period 27 April 2018 – 5 June 2018. Results are
223 presented separately for a full campaign, weekends, and workdays.

Class	Date	Freq _{campaign}	Freq _{weekends}	Freq _{workdays}
Event	5.05, 7.05, 10.05, 13.05, 28.05	12.5%	21%	8%
Non-event	29.04, 1.05, 6.05, 11.05-12.05, 15.05, 21.05, 26.05, 3.06	22.5%	43%	11%
Undefined	27.04-28.04, 30.04, 2.05-4.05, 8.05-9.05, 14.05, 16.05- 20.05, 22.05-25.05, 27.05, 29.05-2.06, 4.06-5.06	65%	36%	81%

224 **3.2. Particle size distributions**

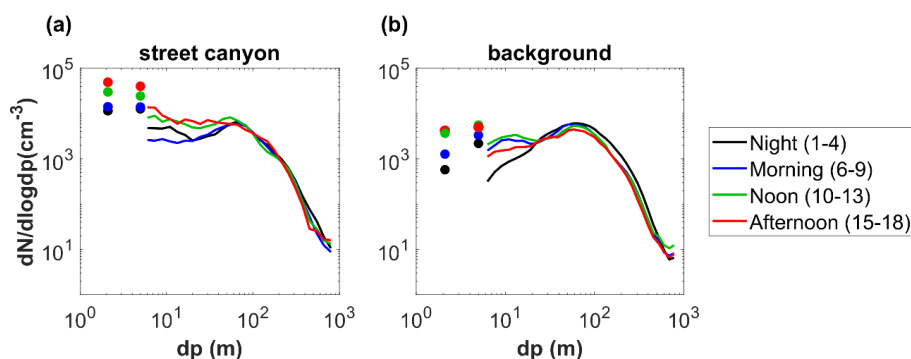


225 Figure 2 presents the median particle size distributions at both stations during workdays and weekends at different times
226 of the day. The shape of the size distributions for Aitken (25-100 nm) and accumulation mode (100-800 nm) particles is
227 quite similar at the two sites, but the concentrations are higher at the street canyon, as discussed later in this section. At
228 the street canyon site, the concentration of particles in a nucleation mode (3-25 nm) has a decreasing trend with an increase
229 of particle size. During the morning, noon, and afternoon, the nucleation mode has a peak below 10 nm, which is
230 characteristic of primary emitted particles from traffic (Rönkkö and Timonen, 2019). Similarly, this peak is observed for
231 nucleation mode particles at the background station during the morning. At the background station, during the night and
232 afternoon, the concentration of particles in nucleation mode increases with increasing particle diameter. During noon the
233 nucleation mode has a peak above 10 nm, likely linked to an NPF event. A sudden change in concentrations of particles
234 with a diameter below and above 7 nm at the background station can be associated with the uncertainty of measurement
235 with different instruments particles smaller than 10 nm (Kangasluoma et al., 2020). The shape of the particle size
236 distribution at the background station is somewhat different from the average size distribution measured at the same
237 location in the years 1997-2003 (Hussein et al., 2004). Hussein et al (2004) found that during spring the size distribution
238 of 8 and 400 nm particles reaches the maximum concentration in the nucleation mode, while in our study concentration
239 of particles within the same size range has a maximum in the Aitken mode. This difference could be explained by a higher
240 contribution of NPF to the average size distribution determined by Hussein et al (2004). At the street canyon site, the
241 shape of the size distribution of larger than 5 nm particles observed in our study is quite similar to the one measured at
242 the same location in May 2017 (Hietikko et al., 2018). In 2017, the particle concentration was observed to reach a
243 maximum for particles around 5 nm (Hietikko et al., 2018), while in our case the highest concentration during daytime is
244 reached for particles smaller than 3 nm.

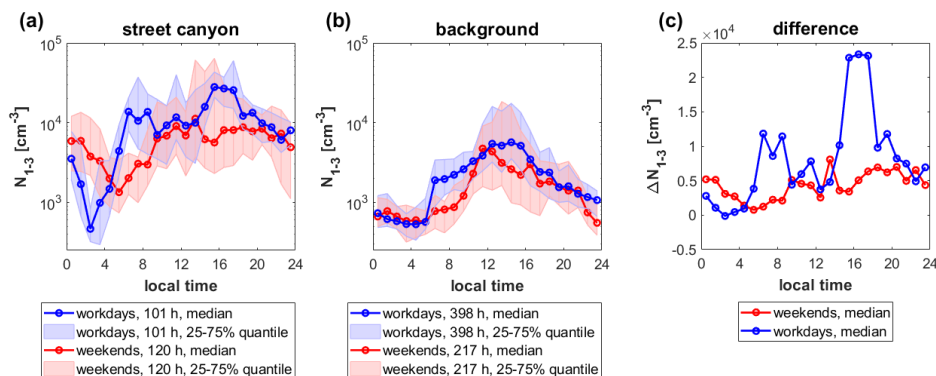
245 Focusing on the smallest particles (Fig. 3), we observe that at the street canyon the median concentration of sub-3 nm
246 particles is up to $2.4 \cdot 10^4 \text{ cm}^{-3}$ higher than at the background station (Fig. 3c). The concentration of sub-3 nm particles is
247 higher at the street canyon site regardless the particle loss due to coagulation scavenging being twice as high as at the
248 background station (discussed later on in this section). At the street canyon, two traffic-related peaks are observed during
249 the morning (6:00-8:00) and afternoon hours (15:00-17:00) on workdays. These peaks correspond to the increase of NOx
250 concentration at the street canyon site during workdays (Fig. S3a). During weekends, there is no morning peak and the
251 afternoon peak occurs earlier (14:00-17:00). The level and the diurnal variations of sub-3 nm particles at the street canyon
252 is similar to observations at the same site in May 2017 by Hietikko et al. (2018). They found that sub-3 nm particles
253 followed the pattern observed in numbers of vehicles at Mäkeläinkatu street. However, in 2017 the morning peak in
254 sub-3 nm particles was shorter and the afternoon peak started one hour earlier. At the background station, the diurnal
255 variation of sub-3 nm particle concentration has a maximum around noon both during weekends and workdays.
256 Nevertheless, a sharp increase of sub-3 nm particles concentration is observed in the morning (6:00) during workdays.
257 Morning raise of sub-3 nm particle concentration at the background station during workdays corresponds to a peak of
258 NOx concentration (Fig. S3b), which suggests the contribution of traffic emissions. The absence of clearly visible
259 traffic-related peaks at the background station could be caused by the 150 m distance of the site uphill from the nearest
260 road as well as the separation of the road and the station by the forest. The midday maximum of sub-3 nm particles
261 concentration is likely related to NPF. However, Kontkanen et al. (2017) showed that at the background station the starting
262 time of a sub-3 nm particle concentration increase varies hardly throughout the year. This means that the increase in
263 sub-3 nm particles concentration is independent of the sunrise, respectively solar radiation. This suggests the partial
264 influence of traffic on the observed peak.



265 The difference between the stations (Fig. 3c) shows that median sub-3 nm particle concentrations during the rush hours
266 in the street canyon site are clearly higher than at the background station throughout, roughly by a factor of 5. However,
267 the concentrations are slightly higher also during other times of the day, which shows the influence of the continuous
268 traffic emissions at the street canyon site.



269 Figure 2. Median size distribution (a) at the street canyon and (b) at the background station. The colors indicate different
270 periods of the day: night (1:00-4:00 LT, black), morning (6:00-9:00 LT, blue), noon (10:00-13:00 LT, green), and
271 afternoon (15:00-18:00, red). Median size distribution was determined by DMPS (particles with sizes between 6-800 nm)
272 marked with solid lines in the figure, UCPC and CPC (3-7 nm), and PSM and UCPC (1-3 nm) marked with dots. This
273 figure with the linear y-axis can be found in Supplementary material (Fig. S2).



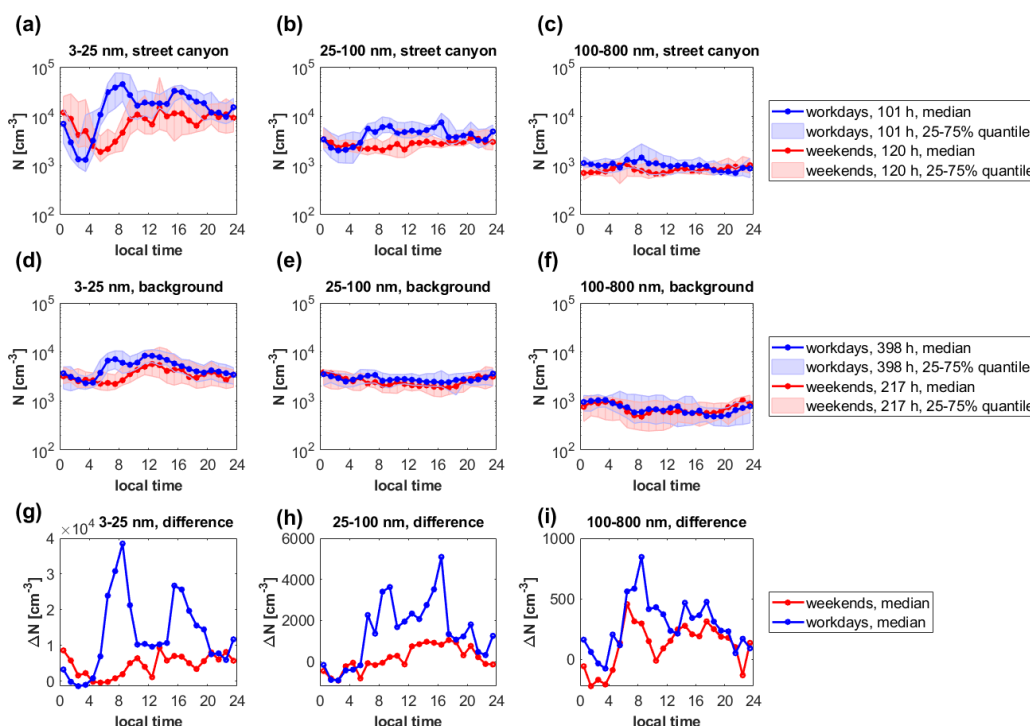
274 Figure 3. The diurnal variation of sub-3 nm particle concentration during weekends (red) and workdays (blue) (a) at the
275 street canyon and (b) at the background station, and (c) the difference between median sub-3 nm particles concentration
276 at the street canyon (a) and at the background station (b). The median diurnal variation is shown as a solid line with
277 markers; the 25th and 75th percentile ranges are presented as shaded areas.
278

279 The diurnal variation of nucleation mode particle concentration is similar to that of sub-3 nm particles at both stations
280 (Fig. 4). During workdays, we can see traffic-related peaks, which are less pronounced on weekends. The concentrations
281 of nucleation mode particles in the street canyon are 10^3 - 3.9×10^4 cm^{-3} higher than at the background station during the
282 daytime. Traffic peaks are also pronounced in the diurnal cycle of Aitken mode particles measured on workdays in the
283 street canyon. Concentrations of Aitken mode particles at the street canyon site are up to 5×10^3 cm^{-3} higher than at the



284 background station on workdays. During nighttime and weekends, concentrations of Aitken mode particles are similar at
285 both stations, which suggests a similar origin of these particles. The diurnal variation of Aitken mode particle
286 concentration at the background station is similar during workdays and weekends, however, during daytime
287 concentrations are higher on workdays. At street canyon during workdays, we can observe traffic-related peak in Aitken
288 mode particles, which are absent during weekends. Accumulation mode particle concentrations during workdays and
289 weekends are comparable at each of the stations (Fig. S4). During daytime accumulation mode particles reached higher
290 concentrations at the street canyon than at the background station, which causes a difference of roughly a factor of two
291 between condensation and coagulation sinks at the sites (Fig. 5). Accumulation mode particle concentration is almost
292 constant during the whole day.

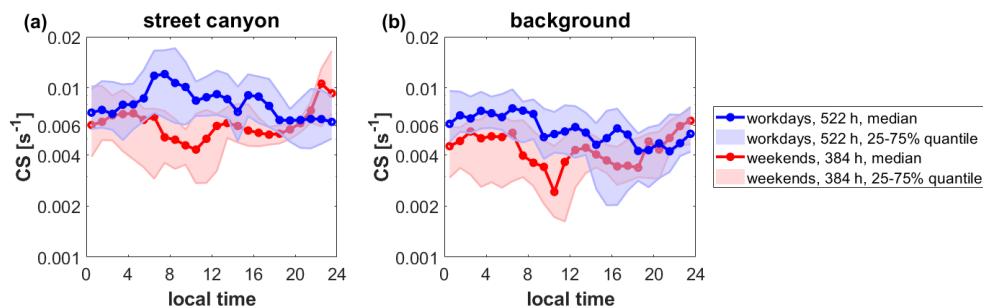
293 Overall, the influence of traffic on the particle population at the street canyon is clearly visible for sub-3 nm, nucleation
294 mode, and Aitken mode particles, while the accumulation mode is only slightly influenced by traffic. The particle
295 concentrations at the background station are also influenced by traffic, but not as strongly as at the street canyon station.
296 At the background station, the influence of traffic can be observed only for sub-3 nm and nucleation mode particles. These
297 results suggest that sub-3 nm and nucleation mode particle concentrations in the urban environment are mainly influenced
298 by local sources, while the accumulation mode particle concentrations are mostly dominated by transport from non-local
299 sources. Whether the Aitken mode is primarily dominated by local or non-local sources depends on the analyzed location.



300
301 Figure 4. Diurnal variations of nucleation (3-25 nm), Aitken (25-100 nm), and accumulation (100-800 nm) modes particle
302 concentration during weekends (red) and workdays (blue) measured at the street canyon (top) and background station
303 (middle) as well as the difference between the street canyon site and the background station concentrations (bottom). The



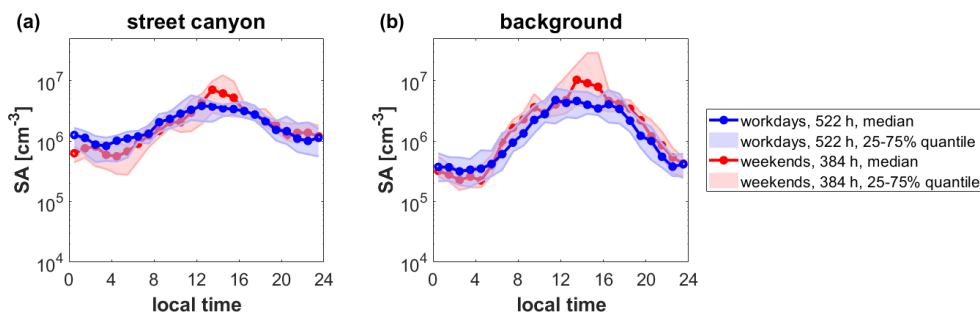
304 median diurnal variations are shown as solid lines with markers; the 25th and 75th percentile ranges are presented as
305 shaded areas. This figure with the linear y-axes can be found in Supplementary material (Fig. S4).



306
307 Figure 5. The diurnal variation of CS during weekends (red) and workdays (blue) (a) at the street canyon and (b) the
308 background station. The median diurnal variation is shown as a solid line with markers; the 25th and 75th percentile range
309 are presented as a shaded area.

310 3.3. Sulfuric acid

311 SA concentration had a clear daytime maximum at both sites (Fig. 6). The only difference in SA concentration between
312 workdays and weekends at each site was observed during midday (13:00-15:00) when SA concentration reached higher
313 values during weekends than weekdays. During weekends, the median SA concentration at the background station had a
314 maximum of $1.1 \cdot 10^7 \text{ cm}^{-3}$ while during workdays, it reached only $4.6 \cdot 10^6 \text{ cm}^{-3}$. A similar pattern is observed at the street
315 canyon station with maximum concentrations of $6.9 \cdot 10^6 \text{ cm}^{-3}$ and $3.6 \cdot 10^6 \text{ cm}^{-3}$ during weekends and weekdays,
316 respectively. This difference is likely linked to a bigger fraction of NPF events days during analyzed weekends than
317 workdays (Table 2). Daytime median SA concentrations are slightly higher at the background station than at the street
318 canyon (Fig. 6, Fig. S5), which is probably caused by higher CS at the street canyon site (Fig. 5). In contrast to daytime,
319 nighttime median SA concentrations are an order of magnitude higher at the street canyon site than at the background
320 station. This difference should not be caused by different instrumental background, as we corrected SA data with zero
321 measurements. High nighttime SA concentration at the street canyon could be caused by direct emission of sulfuric acid
322 from traffic (Arnold et al., 2012) or nighttime SA formation (Guo et al., 2020). SA concentrations at the street canyon
323 site are slightly lower than concentrations measured one year earlier by Olin et al. (2020).



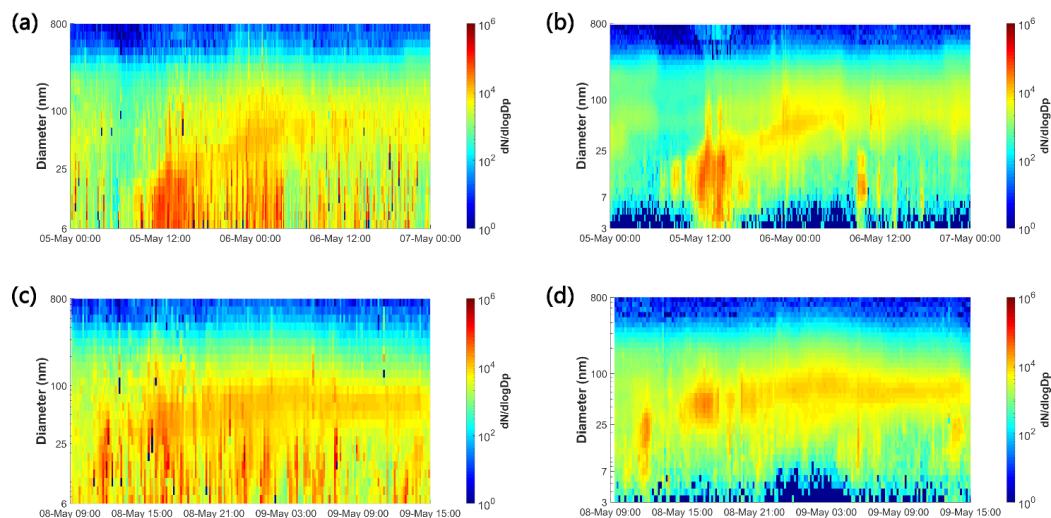
324
325 Figure 6. The diurnal variation of sulfuric acid (SA) concentration (a) at the street canyon and (b) at the background



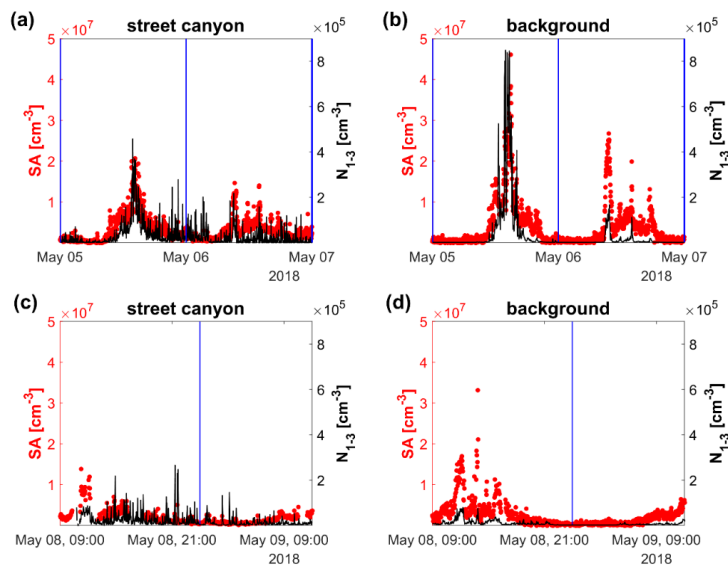
326 station. The median diurnal variation is shown as a solid line with markers; the 25th and 75th percentiles are presented
327 as a shaded area.

328 3.4. Case studies

329 To understand the behavior of sub-3 nm particles on a shorter time scale, we analyzed two periods, when the particle
330 concentration data are available from both sites: Saturday 5 May 2018-Sunday 6 May 2018 and Tuesday 8 May 2018
331 09:00-Wednesday 9 May 2018 15:00. The first investigated case is a weekend starting with an NPF event (Fig. 7a,b). The
332 second case contains typical workdays (Fig. 7c,d), which are classified as undefined days in NPF event classification.
333 Supporting information about atmospheric conditions, trace gas concentrations, black carbon (BC) concentration, and CS
334 during the analyzed cases are presented in Fig. S6-S8. In both studied cases, sub-3 nm particles and SA concentrations
335 follow each other closely at the background station (Fig. 8). Oppositely, at the street canyon site, there are many traffic-
336 related sub-3 nm particles peaks, which often do not have their counterparts in SA time-series. This suggests that the
337 majority of SA is not originating from direct emissions from traffic. Our analysis supports studies showing that sub-3 nm
338 particles are not only formed by clustering of atmospheric vapors, but it is also directly emitted from traffic (Hietikko et
339 al., 2018; Rönkkö et al., 2017; Rönkkö and Timonen, 2019). The pattern of SA time-series is similar at both stations, but
340 SA concentrations are lower at the street canyon. The highest sub-3 nm particles and SA concentrations during both cases
341 were measured at each site during the NPF event. The relation between sub-3 nm particles measured at the street canyon
342 and background station during these case studies is presented in Fig. S9. During the NPF event (Fig. 8a,b), sub-3 nm
343 particles concentration at the background station is almost a factor of two higher than at the street canyon site. However,
344 nearly simultaneous to the highest peak in sub-3 nm particles and SA concentrations, a peak in particle concentrations
345 across the modes (Fig 7b) as well as in SO₂ concentration (Fig. S6) is observed at the background station. This seems not
346 to be a feature of a regional NPF event but could be a plume from e.g. a ship or a coal-fired power plant in Helsinki,
347 which happens to be more efficiently transported to the background station than to the street canyon. This illustrates the
348 interplay of various types of sources on the aerosol concentrations, regional NPF events, local traffic sources, and nearby
349 point sources. It should be kept in mind that this case occurs during the weekend when the traffic volumes are lower and
350 daily patterns of traffic rate differ from weekdays, and thus on average the influence of traffic is expected to be more
351 pronounced.



352 Figure 7. Time series of particle size distribution at the background station (b, d) and at street canyon site (a, c)
 353 measured by DMPS for periods of 5 May 2018–7 May 2018 LT (a, b) and 8 May 2018 09:00–9 May 2018 15:00 LT
 354 (c, d).



355 Figure 8. Time series of sub-3 nm particles (black) and SA (red) concentrations at the street canyon (a, c) and at the
 356 background station (b, d) during 5 May 2018–7 May 2018 LT (a, b) and 8 May 2018 09:00–9 May 2018 15:00 LT (c, d).
 357 Vertical blue lines indicate midnights. This figure with the logarithmic y-axis can be found in Supplementary material
 358 (Fig. S10).

359
 360
 361



362

3.5. Regression analysis

363 To investigate in detail the contribution of different sources to the sub-3 nm particles population at both sites, we analyzed
364 correlations of different variables with sub-3 nm particle concentration (Table 3). Sub-3 nm particle concentration at the
365 background station correlates best with the concentrations of SO₂ (R = 0.64 on workdays and R = 0.46 on weekends) and
366 its oxidation product SA (R = 0.66 on workdays and R = 0.66 on weekends), which is a common precursor of NPF.
367 Sub-3 nm particle concentration at the street canyon correlates best with NO (R = 0.65 on workdays and R = 0.57 on
368 weekends) and NO_x concentrations (R = 0.62 on workdays and R = 0.54 on weekends). Generally, at the street canyon
369 site, high correlations are observed between sub-3 nm particles and species, that can be associated with emissions from
370 traffic: BC, NO_x, NO, CO₂. The correlation between sub-3 nm particles and SA is also positive and high but weaker than
371 at the background station, which is in agreement with results from the case studies. Overall, the correlation analysis
372 suggests that the sub-3 nm particles population at the street canyon site is more influenced by traffic than at the background
373 station. This is discussed more in the next section.

374 Table 3. Correlation between logarithmic values of sub-3 nm particle concentration and logarithmic values of other
375 variables during weekends and workdays at the street canyon and the background station. N shows a number of measured
376 points taken into analysis for each period. In the case of missing data for an analyzed parameter, the number of studied
377 points is shown next to the correlation parameter. All correlations presented in the table are statistically significant at a
378 significance level of $\alpha = 0.05$. Correlations with a Pearson's correlation coefficient higher than 0.5 are marked in bold.

Parameter	Street canyon site		Background station	
	Workdays (N=552)	Weekends (N=696)	Workdays (N=2366)	Weekends (N=1467)
SA [# /cm ³]	0.49	0.61	0.66	0.66
BC [ng/m ³]	0.60	0.33 (N=418)	0.15	0.27
CS [s ⁻¹]	0.29	0.24 (N=418)	-0.10	0.13
NO [ppb]	0.65	0.57	0.37 (N=1813)	0.45 (N=892)
NO _x [ppb]	0.62	0.54	0.28 (N=2218)	0.35 (N=1439)
O ₃ [ppb]	-0.09	-0.24	0.13	0.13
CO ₂ [ppm]	0.38	0.56	-0.24 (N=689)	-0.28 (N=603)
SO ₂ ** [ppb]	-	-	0.64 (N=2051)	0.46 (N=1266)
RH* [%]	-0.43	-0.47	-0.15	-0.11
T* [°C]	0.38	0.45	0.17	0.10
WD* [°]	-0.24	-0.04	-0.20	-0.25

379 * Correlation calculated for logarithmic values of sub-3 nm particle concentration and standard values of the
380 parameter

381

3.6. Estimation of NPF and traffic contribution to sub-3 nm particles

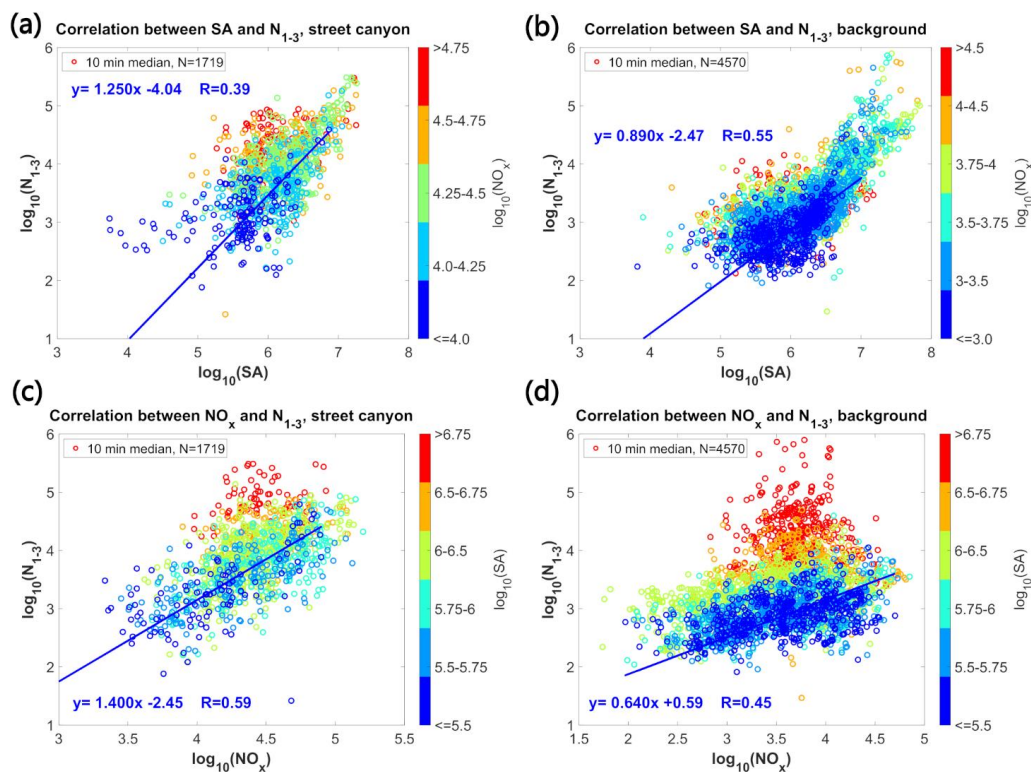
382 Our results suggest that the sub-3 nm particle population at the urban background station is mainly influenced by particles
383 formed by atmospheric NPF, while at the street canyon site it is affected more by particles emitted by traffic. The
384 compounds that correlate best with sub-3 nm particles at each site, SA and NO_x, can be used as markers of NPF and traffic
385 emissions respectively. To quantify the influence of each process on sub-3 nm particle concentrations, we studied the



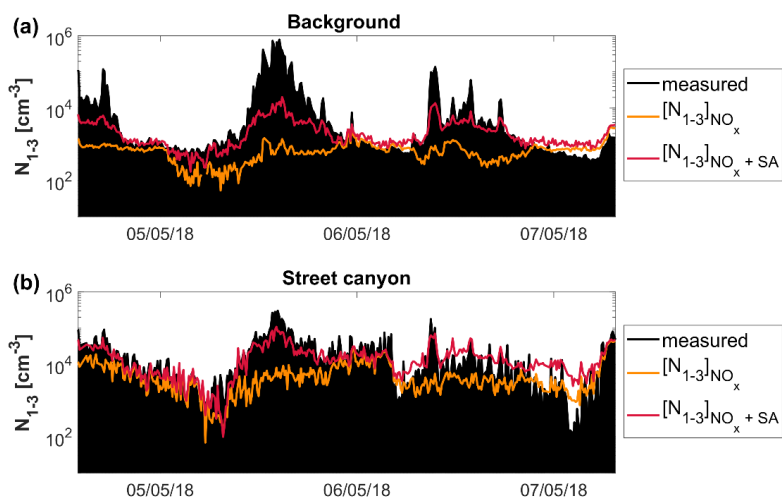
386 dependency between sub-3 nm particles, SA, and NO_x concentrations at both sites (Fig. 9, Table S1). We made bivariate
387 fittings to common logarithms of NO_x and sub-3 nm particles when the SA concentration was low and reversely we
388 analyzed common logarithms of SA and sub-3 nm particles when the NO_x concentration was low. The bins were chosen
389 for fitting so that they were as similar as possible at both stations and contained enough data points. The slopes of the
390 bivariate fit to sub-3 nm particles and SA data for low NO_x concentration is close to 1 at both stations (Fig. 9 a,b). At the
391 same time, the slope of the fit to sub-3 nm particles and NO_x data for low SA concentration is considerably smaller at the
392 background station (0.64) than at the street canyon site (1.40) (Fig. 9 c,d). We investigated possible reasons for this
393 difference such as constant background (local source) of sub-3 nm particles at the background station or losses of sub-
394 3 nm particles due to CS, or particle growth. Analysis of the correlation between NO_x , SA, and total particle concentration
395 (Fig. S11), as well as the correlations between sub-3 nm particles, NO_x , SA, and CS (Fig. S12-S13), implied that neither
396 particle growth out of the sub-3 nm size range nor varying CS can explain the difference in the slopes between stations.
397 One possible explanation could be a constant production of sub-3 nm particles at the background site, as a result of
398 clustering of low-volatile organic vapors (Rose et al., 2018). Comparing ion concentrations and sub-3 nm particles at the
399 background station indicates that the constant source of ions in the atmosphere cannot explain these high sub-3 nm particle
400 concentrations at the background station (Fig. S14). We should have in mind that compared ranges of NO_x concentrations
401 are different at each station. Additionally, particle evaporation may affect the comparison.

402 Based on these bivariate fits, we estimated sub-3 nm particle concentration originating from NPF and traffic at the two
403 sites (Table 4). The analysis was done for the time when NO_x , SA, and sub-3 nm particle concentrations were measured
404 at each station (Table A1, Fig. S15). The variability of estimated sub-3 nm particle concentration is high, and occasionally
405 estimated concentrations exceed the measured values of sub-3 nm particle while at other times estimated values are clearly
406 lower than the measured values (Fig. 10). However, our estimation captures the temporal variation of the sub-3 nm particle
407 concentrations adequately. We can conclude that during the daytime (6:00-20:00), a similar fraction of sub-3 nm particles
408 originate from traffic (53%) and NPF (47%) at the street canyon site. At the background station, the daytime sub-3 nm
409 particle population is dominated by particles originated from NPF (74%). During the nighttime (20:00-6:00), the influence
410 of both sources on the sub-3 nm particles population is almost equal at the background station. At the street canyon site,
411 sub-3 nm particles originate mainly from traffic (65%) during the night. Our estimation of the influence of traffic on sub-
412 3 nm particle population at background station (32%) and street canyon site (54%) agrees with the previous annual
413 estimation of sub-3 nm particles originating by traffic in Helsinki (6-84%) conducted by Olin et al. (2020). Overall, our
414 results are consistent with the fact that the regional NPF process occurs over a large spatial area, while traffic emissions
415 are local.

416 When discussing the estimated relative contribution of traffic and NPF to the sub-3 nm population, we should have in
417 mind that the conducted analysis does not take into account the origin of SA. Traffic can directly or indirectly emit SA,
418 thus traffic may influence SA concentration used for estimating sub-3 nm particles formed during NPF. This could cause
419 an underestimation of the relative contribution of traffic to the sub-3 nm population. Olin et al. (2020) estimated that
420 during May 2017, at typical workday noontime at the same street canyon site, the contribution of traffic to sub-3 nm
421 particles was approximately 85%. The difference between our results and the one presented by Olin et al. (2020) could
422 be partly caused by the influence of traffic to the SA concentration. However, Olin et al. (2020) calculated the traffic
423 contribution to the sub-3 nm particles for a typical workday, while most data (57.8%) from the street canyon site used for
424 our estimation was collected at the time free from work.



425 Figure 9. Correlation between the logarithm of SA and the logarithm of sub-3 nm particles colored by the logarithm of
426 NO_x (a) at the street canyon and (b) at the background station, as well as the correlation between the logarithm of NO_x
427 and the logarithm of sub-3 nm particles colored by the logarithm of SA (c) at the street canyon and (d) at the background
428 station. Blue lines represent bivariate fit done to data with the logarithm of NO_x smaller than 4 at street canyon site (a) or
429 3 at background station (b), or data with the logarithm of SA smaller than 5.5 at both stations (c,d). The parameters of the
430 fit are presented as an equation on the plot.



431 Figure 10. The time series of sub-3 nm particles concentration measured during 4 May 2018-8 May 2018 LT (black) and
 432 estimated based on NO_x concentration (orange) and NO_x and SA concentrations (red) (a) at the background station and
 433 (b) at the street canyon site.

434 Table 4. The percentiles of the relative contributions of traffic and NPF to estimated sub-3 nm particle concentrations at
 435 the background station and the street canyon. [N₁₋₃]_{NO_x} and [N₁₋₃]_{SA} present relative contribution of sub-3 nm particle
 436 concentrations estimated based on NO_x and SA concentrations, representing the contributions of traffic and NPF,
 437 respectively. Equations used for calculating the relative contribution of each source are presented in Appendix
 438 (Eq. A5-A6)

Percentile	[N ₁₋₃] _{NO_x}			[N ₁₋₃] _{SA}		
	25	50	75	25	50	75
Daytime						
Background [%]	9	26	30	70	74	91
Street canyon [%]	26	47	70	30	53	74
Nighttime						
Background [%]	41	67	75	25	33	59
Street canyon [%]	38	65	86	14	35	62
All campaign						
Background [%]	14	43	57	43	57	86
Street canyon [%]	32	54	78	22	46	68

439 4. Conclusions

440 In this study, for the first time, the particle size distribution in a diameter range from 1 to 800 nm was analyzed at two
 441 close-by stations in Helsinki. We found that the influence of traffic on particle number concentrations at the street canyon
 442 is most visible for sub-3 nm, nucleation mode, and Aitken mode particles, while at the background station the influence



443 of traffic is clear only for sub-3 nm and nucleation mode particles. Sub-3 nm and nucleation mode particles are influenced
444 by local sources, especially traffic, while accumulation mode particles are dominated by long-range transportation from
445 non-local sources. Whether Aitken mode particles are more influenced by local or non-local sources, depends on the
446 location. At the background station, Aitken mode is largely dominated by non-local sources, while at the street canyon
447 site this mode is influenced by traffic.

448 We observed a very similar pattern in diurnal variation of SA concentration at both stations. Daytime SA concentrations
449 were slightly higher at the background station, likely due to a lower condensation sink than at the street canyon site.
450 During the nighttime, SA concentration was almost an order of magnitude higher at the street station. High nighttime
451 concentration at the street canyon site is probably caused by two simultaneous processes: direct SA emission from traffic
452 and nighttime SA formation.

453 Additionally, we performed two case studies, in which we analyzed the variation of SA and sub-3 nm particles on a short
454 time scale. Our study supports previous research showing that sub-3 nm particles include direct emissions from traffic.
455 During the NPF event on 5 May 2018, sub-3 nm particle concentrations at both sites were the highest, and traffic
456 contribution to the total sub-3 nm particle concentration at the analyzed stations was small.

457 Furthermore, we analyzed the relation of sub-3 nm particles with trace gases and meteorological variables. We observed
458 that sub-3 nm particles at the background station are mainly related to SO₂ and SA, while the sub-3 nm particle population
459 at the street canyon can be associated with components linked to traffic emissions (BC, NO_x, NO, and CO₂). Based on
460 these observations, we developed a new method to estimate the relative contributions of traffic and NPF to sub-3 nm
461 particle concentration at nearby urban sites. The relative impacts of traffic and NPF on the sub-3 nm particles in the urban
462 environment have not been quantified before. The results of our estimates suggest that NPF has a stronger influence on
463 the sub-3 nm particle population than traffic at the urban background site, especially during the daytime. At the street
464 canyon site, NPF and traffic contribute to sub-3 nm concentrations rather equally. This indicates that traffic is an important
465 source of sub-3 nm particles, but it does not solely dominate the sub-3 nm particle population at either of the studied sites
466 in Helsinki during the daytime in spring. However, in our estimation, we considered only the process of formation or
467 emission of sub-3 nm particles, and thus we did not account for the origin of NPF precursors. SA, as well as other low-
468 volatile compounds, can be emitted by traffic and then participate in the formation of sub-3 nm particles. Furthermore,
469 one should note that this estimation is performed only with a limited data set, and therefore it may not provide a full
470 picture of the contributions of NPF and traffic to sub-3 nm particles in Helsinki. The relations between emissions of
471 particles and NO_x from traffic and between NPF and SA are expected to vary seasonally or as a function of temperature
472 (Gidhagen et al., 2005; Nieminen et al., 2014) and, consequently, the parameters derived in this study are not expected to
473 be valid through the year in Helsinki, even less in other locations. For instance, NPF events are frequently observed in
474 Finland in spring and autumn but very seldom in winter (Hussein et al., 2008), and particle emissions from traffic are
475 expected to be higher during colder temperatures in winter (Gidhagen et al., 2005). Since this study was conducted in
476 spring, the role of NPF events as a sub-3 nm particles source would probably be much smaller in winter.

477 Future studies should focus on different low-volatile compounds in an urban environment and investigate their influence
478 on NPF. Additionally, analyzing the relative influence of different processes on the sub-3 nm particle population based
479 on long-term measurements would be beneficial. In the future, the method developed in this study can also be applied to
480 estimate the contribution of traffic to particle number concentrations in other urban environments. This knowledge can
481 contribute to a better understanding of the effects of traffic on air quality and human health.



482 **Appendix**

483 Table A1. Working time of instruments used during the campaign.

Instrument	Model	Working period	Working time [h]
Street canyon			
Particle Size Magnifier (PSM) fixed mode	Airmodus A11 nCNC	27.04.2018 13:00 – 02.05.2018 08:00 04.05.2018 09:00 – 07.05.2018 15:00 08.05.2018 10:00 – 09.05.2018 14:00 10.05.2018 10:00 – 10.05.2018 14:00 11.05.2018 01:00 – 11.05.2018 17:00	246
PSM step mode	Airmodus A11 nCNC	27.04.2018 00:00 – 15.05.2018 12:00 15.05.2018 21:00 – 01.05.2018 00:00	833
Ultrafine Condensation Particle Counter (UCPC)	TSI 3776	27.04.2018 14:00 – 30.04.2018 07:00 03.05.2018 19:00 – 06.05.2018 09:00 08.05.2018 11:00 – 18.05.2018 16:00 21.05.2018 18:00 – 21.05.2018 22:00 24.05.2018 10:00 – 24.05.2018 12:00 24.05.2018 16:00 – 31.05.2018 10:00	548
Condensation Particle Counter A20 (CPC)	Airmodus A20	27.04.2018 14:00 – 17.05.2018 15:00 17.05.2018 23:00 – 22.05.2018 10:00 24.05.2018 10:00 – 25.05.2018 14:00 26.05.2018 00:00 – 31.05.2018 10:00	750
Differential Mobility Particle Sizer (DMPS)	Vienna-type DMA coupled with Airmodus A20 DMA	27.04.2018 00:00 – 31.05.2018 23:00	840
Atmospheric Pressure Interface Time-Of-Flight Mass Spectrometer with the Chemical Ionization (CI-API-TOF)	TOFWERK AG	02.05.2018 00:00 – 03.05.2018 13:00 04.05.2018 15:00 – 08.05.2018 09:00 08.05.2018 13:00 – 08.05.2018 15:00 08.05.2018 18:00 – 10.05.2018 09:00 10.05.2018 12:00 – 16.05.2018 09:00 16.05.2018 12:00 – 22.05.2018 10:00 22.05.2018 12:00 – 24.05.2018 07:00	501
SO ₂ analyzer	43i-TLE	09.05.2018 12:00 – 10.05.2018 17:00 11.05.2018 09:00 – 11.05.2018 18:00 14.05.2018 09:00 – 31.05.2018 12:00	452
CO ₂ analyzer	LI-COR LI-7000	27.04.2018 09:00 – 24.05.2018 13:00 24.05.2018 16:00 – 29.05.2018 19:00	771
CO ₂ analyzer (Tut)		17.05.2018 14:00 – 19.05.2018 00:00 21.05.2018 17:00 – 21.05.2018 20:00 24.05.2018 10:00 – 24.05.2018 11:00	90



		25.05.2018 12:00 – 25.05.2018 13:00 28.05.2018 10:00 – 28.05.2018 14:00 28.05.2018 16:00 – 29.05.2018 08:00 30.05.2018 11:00 – 31.05.2018 10:00	
Background			
PSM fixed mode	Airmodus A11 nCNC	01.05.2018 10:00 – 10.05.2018 04:00 11.05.2018 08:00 – 05.06.2018 10:00	766
PSM scanning mode	Airmodus A11 nCNC	04.05.2018 00:00 – 21.05.2018 11:00 21.05.2018 22:00 – 30.05.2018 05:00 02.06.2018 22:00 – 05.06.2018 00:00	671
UCPC	TSI 3776	03.05.2018 17:00 – 10.05.2018 04:00 11.05.2018 08:00 – 21.05.2018 16:00 25.05.2018 10:00 – 05.06.2018 10:00	670
CPC	Airmodus A20	03.05.2018 11:00 – 10.05.2018 04:00 11.05.2018 08:00 – 20.05.2018 00:00 21.05.2018 14:00 – 05.06.2018 10:00	728
Twin Differential Mobility Particle Sizer (Twin-DMPS)		01.05.2018 01:00 – 07.05.2018 14:00 08.05.2018 09:00 – 05.06.2018 00:00	821
Neutral and Air Ion Spectrometer (NAIS)	Airel Ltd	26.04.2018 13:00 – 17.05.2018 02:00 18.05.2018 21:00 – 06.06.2018 02:00	932
CI-API-TOF	TOFWERK AG	02.05.2018 15:00 – 04.06.2018 00:00	776
SO ₂ analyzer		27.04.2018 01:00 – 07.05.2018 12:00 08.05.2018 11:00 – 06.06.2018 00:00	937
CO ₂ analyzer		03.05.2018 18:00 – 14.05.2018 01:00	248

484 Table A2. Overview of additional variables used in this study measured at the background station and the street canyon
 485 site.

Variable [unit]	Instrument / model	Height (m)
Background station		
NO, NO _x [ppb]	chemiluminescence analyzer / Horiba APNA 370	4
O ₃	UV-absorption / Teledyne Instruments API 400E	4
SO ₂ [ppb]	UV fluorescence analyzer / Thermo Fisher Scientific TEI 43iTLE	4
Relative humidity [%]	Vaisala HMP243	29
Air temperature [°C]	Pentronic Pt100	4
Wind direction [°]	2D ultrasonic anemometer/ Thies Clima 2.1x	32
Wind speed [m/s]	2D ultrasonic anemometer/ Thies Clima 2.1x	32
Global radiation [W/m ²]	Kipp and Zonen CNR1	32



Black carbon	Multi Angle Absorption Photometer (MAAP), Thermo Scientific, Model 5012	4
Ion size distribution [cm ⁻³]	neutral cluster and air ion spectrometer (NAIS)	1.5
Street canyon		
NO, NO _x [μg/m ³]	chemiluminescence analyzer / Horiba APNA 370	4
O ₃ [μg/m ³]	UV fluorescence analyzer / Horiba APOA-370	4
Relative humidity [%]	Vaisala WXT 536	4
Air temperature [°C]	Vaisala WXT 536	4
Wind direction [°]	Vaisala WXT 536	4
Wind speed [m/s]	Vaisala WXT 536	4
Black carbon	Optical analyzer / MAAP 5012	4

486 Calculating the relative contribution of traffic and NPF to sub-3 nm particle population

487 Based on bivariate fittings on the common logarithms of sub-3 nm particles and SA when NO_x concentration was low at
 488 the street canyon site (Fig. 9a), we determined Eq. A1 estimating the concentration of sub-3 nm particles formed during
 489 NPF ($[N_{1-3}]_{SA}$) at the street canyon site. The same analysis conducted for the concentrations at the background station
 490 (Fig. 9b) resulted in Eq. A2. Correlation between common logarithms of sub-3 nm particles and NO_x, when SA
 491 concentration was low, at the street canyon and background station (Fig. 9c-d) was used to determine Eq. A3 and A4,
 492 respectively. Equations A3 and A4 estimate the concentration of sub-3 nm particles emitted from traffic ($[N_{1-3}]_{NO_x}$).

$$[N_{1-3}]_{SA} = 10^{-4.04} \cdot [SA]^{1.25} \quad (\text{street canyon}) \quad (\text{A1})$$

where $[N_{1-3}]_{SA}$ is an estimated concentration of sub-3 nm particles formed during NPF, and $[SA]$ is a SA concentration.

$$[N_{1-3}]_{SA} = 10^{-2.86} \cdot [SA]^{0.99} \quad (\text{background}) \quad (\text{A2})$$

$$[N_{1-3}]_{NO_x} = 10^{-2.45} \cdot [NO_x]^{1.40} \quad (\text{street canyon}) \quad (\text{A3})$$

where $[N_{1-3}]_{NO_x}$ an estimated concentration of sub-3 nm particles emitted from traffic, and $[NO_x]$ is a NO_x concentration.

$$[N_{1-3}]_{NO_x} = 10^{0.59} \cdot [NO_x]^{0.64} \quad (\text{background}) \quad (\text{A4})$$

493 Based on Eq. A1-A4, the relative contribution of traffic and NPF at each site was computed. To calculate the relative
 494 contribution of traffic ($x_{[N_{1-3}]_{NO_x}}$), the estimated concentration of sub-3 nm particles emitted by traffic was divided by
 495 the sum of estimated concentrations of sub-3 nm particles emitted by traffic and formed during NPF (Eq. A5). Similarly,
 496 the relative contribution of NPF ($x_{[N_{1-3}]_{SA}}$) was computed by dividing the estimated concentration of sub-3 nm particles
 497 formed during NPF by the sum of estimated concentrations of sub-3 nm particles emitted by traffic and formed during
 498 NPF (Eq. A6). The relative contribution of each source was calculated for the street canyon and the background station.

$$x_{[N_{1-3}]_{NO_x}} = \frac{[N_{1-3}]_{NO_x}}{[N_{1-3}]_{SA} + [N_{1-3}]_{NO_x}} \cdot 100\% \quad (\text{A5})$$



where $x_{[N_{1-3}]NO_x}$ is a relative contribution of traffic, $[N_{1-3}]NO_x$ is an estimated concentration of sub-3 nm particles emitted by traffic, and $[N_{1-3}]SA$ is an estimated concentration of sub-3 nm particles formed during NPF.

$$x_{[N_{1-3}]SA} = \frac{[N_{1-3}]SA}{[N_{1-3}]SA + [N_{1-3}]NO_x} \cdot 100\% \quad (A6)$$

where $x_{[N_{1-3}]SA}$ is a relative contribution of NPF, $[N_{1-3}]NO_x$ is an estimated concentration of sub-3 nm particles emitted by traffic, and $[N_{1-3}]SA$ is an estimated concentration of sub-3 nm particles formed during NPF.

499 **Data availability**

500 Data will be published in an open data repository. DMPS, BC, O₃, meteorological data measured at the background station
501 are available at the SmartSMEAR data repository (<https://avaa.tdata.fi/web/smart>).

502 **Author contribution**

503 The main ideas were formulated by TP, PP, JKo, HK, JVN and the results were interpreted by MOK, JKo, HK, PP, and
504 TR. HK, MA, KT, HL, LS prepared measurement methodology and OG, HK, MOI, RB, HP, MA, HL, and LS contributed
505 to data collection. MOK, HK, KT, RB performed the data analysis. Instruments were calibrated by MOI, JKa, YJT, and
506 RB. MS, TP, TR, HT, JVN coordinated project while JKo, OG, PP, JKa, and HT supervised it. MS, TP, HT, TR made a
507 funding acquisition. MOK visualized data and prepared the manuscript with contributions from other authors. All the
508 authors reviewed the manuscript.

509 **Competing interests**

510 The authors declare that they have no conflict of interest.

511 **Acknowledgments.**

512 This research was supported by the Regional innovations and experimentations funds AIKO (project HAQT, AIKO014),
513 Business Finland (CITYZER project, Tekes nro: 3021/31/2015 and 2883/31/2015), Pegasor Oy and HSY, Academy of
514 Finland (grant nos 273010, 307331, 310626, 311932, 316114, 318940, 1325656 & 326437), Healthy Outdoor Premises
515 for Everyone (HOPE), Urban Innovation Actions, Regional development funds, University of Helsinki doctoral
516 programme (ATM-DP) and Faculty of Science 3-year grant (75284132), Tampere University of Technology graduate
517 school, and ERA-PLANET project SMURBS (Grant Agreement 689443) under the EU Horizon 2020 Framework.

518 We would like to thank the people who took care of instruments and measurements at the SMEAR III (Pekka Rantala,
519 Erkki Siivola, Pasi Aalto, Petri Keronen, Frans Korhonen, Tiia Laurila, Lauriane Quéléver, Tuuli Lehmusjärvi, Deniz
520 Kempainen) and the HSY Mäkelänkatu site (Anssi Julkunen, Anders Svens, Taneli Mäkelä, Tommi Wallenius, Anu
521 Kousa). In addition, we thank Jiali Shen and Xucheng He for help with the calibration of CI-API-TOF and Lei Yao for
522 useful discussions.

523 **References**

524 André, N.: Air Pollution – Related Illness: Effects of Particles, *Science* (80-.), 804(2005),
525 doi:10.1126/science.1108752, 2014.

526 Andreae, M. O.: Correlation between cloud condensation nuclei concentration and aerosol optical thickness in remote



- 527 and polluted regions, *Atmos. Chem. Phys.*, 9(2), 543–556, doi:10.5194/acp-9-543-2009, 2009.
- 528 Arnold, F., Pirjola, L., Rönkkö, T., Reichl, U., Schlager, H., Lähde, T., Heikkilä, J. and Keskinen, J.: First online
529 measurements of sulfuric acid gas in modern heavy-duty diesel engine exhaust: Implications for nanoparticle formation,
530 *Environ. Sci. Technol.*, 46(20), 11227–11234, doi:10.1021/es302432s, 2012.
- 531 Bousiotis, D., Dall’Osto, M., Beddows, D. C. S., Pope, F. D. and Harrison, R. M.: Analysis of new particle
532 formation (NPF) events at nearby rural, urban background and urban roadside sites, *Atmos. Chem. Phys.*, 19(8), 5679–
533 5694, doi:10.5194/acp-19-5679-2019, 2019.
- 534 Cantrell, C. A.: Technical Note: Review of methods for linear least-squares fitting of data and application to
535 atmospheric chemistry problems, *Atmos. Chem. Phys.*, 8(17), 5477–5487, doi:10.5194/acp-8-5477-2008, 2008.
- 536 Dal Maso, M., Kulmala, M., Riipinen, I., Wagner, R., Hussein, T., Aalto, P. P. and Lehtinen, K. E. J.: Formation and
537 growth of fresh atmospheric aerosols: Eight years of aerosol size distribution data from SMEAR II, Hyytiälä, Finland,
538 *Boreal Environ. Res.*, 10(5), 323–336, 2005.
- 539 Deventer, M. J., von der Heyden, L., Lamprecht, C., Graus, M., Karl, T. and Held, A.: Aerosol particles during the
540 Innsbruck Air Quality Study (INNAQS): Fluxes of nucleation to accumulation mode particles in relation to selective
541 urban tracers, *Atmos. Environ.*, 190, 376–388, doi:10.1016/j.atmosenv.2018.04.043, 2018.
- 542 Ehn, M., Thornton, J. A., Kleist, E., Sipilä, M., Junninen, H., Pullinen, I., Springer, M., Rubach, F., Tillmann, R., Lee,
543 B., Lopez-Hilfiker, F., Andres, S., Acir, I. H., Rissanen, M., Jokinen, T., Schobesberger, S., Kangasluoma, J.,
544 Kontkanen, J., Nieminen, T., Kurtén, T., Nielsen, L. B., Jørgensen, S., Kjaergaard, H. G., Canagaratna, M., Maso, M.
545 D., Berndt, T., Petäjä, T., Wahner, A., Kerminen, V. M., Kulmala, M., Worsnop, D. R., Wildt, J. and Mentel, T. F.: A
546 large source of low-volatility secondary organic aerosol, *Nature*, 506(7489), 476–479, doi:10.1038/nature13032, 2014.
- 547 Eisele, F. L. and Tanner, D. J.: Measurement of the gas phase concentration of H₂SO₄ and methane sulfonic acid and
548 estimates of H₂SO₄ production and loss in the atmosphere, *J. Geophys. Res.*, 98(D5), 9001–9010,
549 doi:10.1029/93JD00031, 1993.
- 550 Fu, Y., Xue, M., Cai, R., Kangasluoma, J. and Jiang, J.: Theoretical and experimental analysis of the core sampling
551 method: Reducing diffusional losses in aerosol sampling line, *Aerosol Sci. Technol.*, 53(7), 793–801,
552 doi:10.1080/02786826.2019.1608354, 2019.
- 553 Geels, C., Andersson, C., Hänninen, O., Lansø, A., Schwarze, P., Skjøth, C. and Brandt, J.: Future Premature Mortality
554 Due to O₃, Secondary Inorganic Aerosols and Primary PM in Europe — Sensitivity to Changes in Climate,
555 Anthropogenic Emissions, Population and Building Stock, *Int. J. Environ. Res. Public Health*, 12(3), 2837–2869,
556 doi:10.3390/ijerph120302837, 2015.
- 557 Gidhagen, L., Johansson, C., Langner, J. and Foltescu, V. L.: Urban scale modeling of particle number concentration in
558 Stockholm, *Atmos. Environ.*, 39(9), 1711–1725, doi:10.1016/j.atmosenv.2004.11.042, 2005.
- 559 Guo, Y., Yan, C., Li, C., Feng, Z., Zhou, Y., Lin, Z., Dada, L., Stolzenburg, D., Yin, R., Kontkanen, J., Daellenbach,
560 K., Kangasluoma, J., Yao, L., Chu, B., Wang, Y., Cai, R., Bianchi, F., Liu, Y. and Kulmala, M.: Formation of
561 Nighttime Sulfuric Acid from the Ozonolysis of Alkenes in Beijing, *Atmos. Chem. Phys.*, 1–18, doi:10.5194/acp-2019-



- 562 1111, 2020.
- 563 Harrison, R. M., Beddows, D. C. S., Alam, M. S., Singh, A., Brean, J., Xu, R., Kotthaus, S. and Grimmond, S.:
564 Interpretation of particle number size distributions measured across an urban area during the FASTER campaign,
565 *Atmos. Chem. Phys.*, 19(1), 39–55, doi:10.5194/acp-19-39-2019, 2019.
- 566 Hietikko, R., Kuuluvainen, H., Harrison, R. M., Portin, H., Timonen, H., Niemi, J. V. and Rönkkö, T.: Diurnal variation
567 of nanocluster aerosol concentrations and emission factors in a street canyon, *Atmos. Environ.*, 189(March), 98–106,
568 doi:10.1016/j.atmosenv.2018.06.031, 2018.
- 569 Hofman, J., Staelens, J., Cordell, R., Stroobants, C., Zikova, N., Hama, S. M. L., Wyche, K. P., Kos, G. P. A., Van Der
570 Zee, S., Smallbone, K. L., Weijers, E. P., Monks, P. S. and Roekens, E.: Ultrafine particles in four European urban
571 environments: Results from a new continuous long-term monitoring network, *Atmos. Environ.*, 136, 68–81,
572 doi:10.1016/j.atmosenv.2016.04.010, 2016.
- 573 Hussein, T., Puustinen, A., Aalto, P. P., Mäkelä, J. M., Hämeri, K. and Kulmala, M.: Urban aerosol number size
574 distributions, *Atmos. Chem. Phys.*, 4(2), 391–411, doi:10.5194/acp-4-391-2004, 2004.
- 575 Hussein, T., Karppinen, A., Kukkonen, J., Härkönen, J., Aalto, P. P., Hämeri, K., Kerminen, V. M. and Kulmala, M.:
576 Meteorological dependence of size-fractionated number concentrations of urban aerosol particles, *Atmos. Environ.*,
577 40(8), 1427–1440, doi:10.1016/j.atmosenv.2005.10.061, 2006.
- 578 Hussein, T., Martikainen, J., Junninen, H., Sogacheva, L., Wagner, R., Dal Maso, M., Riipinen, I., Aalto, P. P.,
579 Kulmala, M., Maso, M. D., Riipinen, I., Aalto, P. P. and Kulmala, M.: Observation of regional new particle formation
580 in the urban atmosphere, *Tellus, Ser. B Chem. Phys. Meteorol.*, 60(4), 509–521, doi:10.1111/j.1600-
581 0889.2008.00365.x, 2008.
- 582 Hussein, T., Junninen, H., Tunved, P., Kristensson, A., Dal Maso, M., Riipinen, I., Aalto, P. P., Hansson, H. C.,
583 Swietlicki, E. and Kulmala, M.: Time span and spatial scale of regional new particle formation events over Finland and
584 Southern Sweden, *Atmos. Chem. Phys.*, 9(14), 4699–4716, doi:10.5194/acp-9-4699-2009, 2009.
- 585 Hyslop, N. P.: Impaired visibility: the air pollution people see, *Atmos. Environ.*, 43(1), 182–195,
586 doi:10.1016/j.atmosenv.2008.09.067, 2009.
- 587 Im, U., Brandt, J., Geels, C., Hansen, K. M., Christensen, J. H., Andersen, M. S., Solazzo, E., Kioutsioukis, I., Alyuz,
588 U., Balzarini, A., Baro, R., Bellasio, R., Bianconi, R., Bieser, J., Colette, A., Curci, G., Farrow, A., Flemming, J.,
589 Fraser, A., Jimenez-Guerrero, P., Kitwiroon, N., Liang, C.-K., Nopmongkol, U., Pirovano, G., Pozzoli, L., Prank, M.,
590 Rose, R., Sokhi, R., Tuccella, P., Unal, A., Vivanco, M. G., West, J., Yarwood, G., Hogrefe, C. and Galmarini, S.:
591 Assessment and economic valuation of air pollution impacts on human health over Europe and the United States as
592 calculated by a multi-model ensemble in the framework of AQMEII3, *Atmos. Chem. Phys.*, 18(8), 5967–5989,
593 doi:10.5194/acp-18-5967-2018, 2018.
- 594 Im, U., Christensen, J. H., Nielsen, O.-K. K., Sand, M., Makkonen, R., Geels, C., Anderson, C., Kukkonen, J., Lopez-
595 Aparicio, S. and Brandt, J.: Contributions of Nordic anthropogenic emissions on air pollution and premature mortality
596 over the Nordic region and the Arctic, *Atmos. Chem. Phys.*, 19(20), 12975–12992, doi:10.5194/acp-19-12975-2019,
597 2019.



- 598 Järvi, L., Hannuniemi, H., Hussein, T., Junninen, H., Aalto, P. P., Hillamo, R., Mäkelä, T., Keronen, P., Siivola, E.,
599 Vesala, T. and Kulmala, M.: The urban measurement station SMEAR III: Continuous monitoring of air pollution and
600 surface-atmosphere interactions in Helsinki, Finland, *Boreal Environ. Res.*, 14(SUPPL. A), 86–109, 2009.
- 601 Jiang, J., Chen, M., Kuang, C., Attoui, M. and McMurry, P. H.: Electrical Mobility Spectrometer Using a Diethylene
602 Glycol Condensation Particle Counter for Measurement of Aerosol Size Distributions Down to 1 nm, *Aerosol Sci.*
603 *Technol.*, 45(4), 510–521, doi:10.1080/02786826.2010.547538, 2011.
- 604 Jokinen, T., Sipilä, M., Junninen, H., Ehn, M., Lönn, G., Hakala, J., Petäjä, T., Mauldin, R. L., Kulmala, M., Worsnop,
605 D. R., Mauldin III, R. L., Kulmala, M. and Worsnop, D. R.: Atmospheric sulphuric acid and neutral cluster
606 measurements using CI-API-TOF, *Atmos. Chem. Phys.*, 12(9), 4117–4125, doi:10.5194/acp-12-4117-2012, 2012.
- 607 Junninen, H., Ehn, M., Petäjä, T., Luosujärvi, L., Kotiaho, T., Kostiainen, R., Rohner, U., Gonin, M., Fuhrer, K.,
608 Kulmala, M. and Worsnop, D. R.: A high-resolution mass spectrometer to measure atmospheric ion composition,
609 *Atmos. Meas. Tech.*, 3(4), 1039–1053, doi:10.5194/amt-3-1039-2010, 2010.
- 610 Kangasluoma, J. and Attoui, M.: Review of sub-3 nm condensation particle counters, calibrations, and cluster
611 generation methods, *Aerosol Sci. Technol.*, 53(11), 1277–1310, doi:10.1080/02786826.2019.1654084, 2019.
- 612 Kangasluoma, J. and Kontkanen, J.: On the sources of uncertainty in the sub-3 nm particle concentration measurement,
613 *J. Aerosol Sci.*, 112, 34–51, doi:10.1016/j.jaerosci.2017.07.002, 2017.
- 614 Kangasluoma, J., Junninen, H., Lehtipalo, K., Mikkilä, J., Vanhanen, J., Attoui, M., Sipilä, M., Worsnop, D., Kulmala,
615 M. and Petäjä, T.: Remarks on ion generation for CPC detection efficiency studies in sub-3-nm size range, *Aerosol Sci.*
616 *Technol.*, 47(5), 556–563, doi:10.1080/02786826.2013.773393, 2013.
- 617 Kangasluoma, J., Kuang, C., Wimmer, D., Rissanen, M. P., Lehtipalo, K., Ehn, M., Worsnop, D. R., Wang, J., Kulmala,
618 M. and Petäjä, T.: Sub-3 nm particle size and composition dependent response of a nano-CPC battery, *Atmos. Meas.*
619 *Tech.*, 7(3), 689–700, doi:10.5194/amt-7-689-2014, 2014.
- 620 Kangasluoma, J., Attoui, M., Junninen, H., Lehtipalo, K., Samodurov, A., Korhonen, F., Sarnela, N., Schmidt-Ott, A.,
621 Worsnop, D., Kulmala, M. and Petäjä, T.: Sizing of neutral sub 3nm tungsten oxide clusters using Airmodus Particle
622 Size Magnifier, *J. Aerosol Sci.*, 87, 53–62, doi:10.1016/j.jaerosci.2015.05.007, 2015.
- 623 Kangasluoma, J., Samodurov, A., Attoui, M., Franchin, A., Junninen, H., Korhonen, F., Kurtén, T., Vehkamäki, H.,
624 Sipilä, M., Lehtipalo, K., Worsnop, D. R., Petäjä, T. and Kulmala, M.: Heterogeneous Nucleation onto Ions and
625 Neutralized Ions: Insights into Sign-Preference, *J. Phys. Chem. C*, 120(13), 7444–7450, doi:10.1021/acs.jpcc.6b01779,
626 2016.
- 627 Kangasluoma, J., Hering, S., Picard, D., Lewis, G., Enroth, J., Korhonen, F., Kulmala, M., Sellegri, K., Attoui, M. and
628 Petäjä, T.: Characterization of three new condensation particle counters for sub-3 nm particle detection during the
629 Helsinki CPC workshop: The ADI versatile water CPC, TSI 3777 nano enhancer and boosted TSI 3010, *Atmos. Meas.*
630 *Tech.*, 10(6), 2271–2281, doi:10.5194/amt-10-2271-2017, 2017.
- 631 Kangasluoma, J., Cai, R., Jiang, J., Deng, C., Stolzenburg, D., Ahonen, L. R., Chan, T., Fu, Y., Kim, C., Laurila, T. M.,
632 Zhou, Y., Dada, L., Sulo, J., Flagan, R. C., Kulmala, M., Petäjä, T. and Lehtipalo, K.: Overview of measurements and



- 633 current instrumentation for 1–10 nm aerosol particle number size distributions, *J. Aerosol Sci.*, 148(November 2019),
634 1–29, doi:10.1016/j.jaerosci.2020.105584, 2020.
- 635 Kangasniemi, O., Kuuluvainen, H., Heikkilä, J., Pirjola, L., Niemi, J. V., Timonen, H., Saarikoski, S., Rönkkö, T., Dal
636 Maso, M. and Maso, M. D.: Dispersion of a traffic related nanocluster aerosol near a major road, *Atmosphere (Basel)*,
637 10(6), 1–19, doi:10.3390/atmos10060309, 2019.
- 638 Kerminen, V.-M., Chen, X., Vakkari, V., Petäjä, T., Kulmala, M. and Bianchi, F.: Atmospheric new particle formation
639 and growth: review of field observations, *Environ. Res. Lett.*, 13(10), 103003, doi:10.1088/1748-9326/aadf3c, 2018.
- 640 Kontkanen, J., Lehtipalo, K., Ahonen, L., Kangasluoma, J., Manninen, H. E., Hakala, J., Rose, C., Sellegri, K., Xiao, S.,
641 Wang, L., Qi, X., Nie, W., Ding, A., Yu, H., Lee, S., Kerminen, V.-M., Petäjä, T. and Kulmala, M.: Measurements of
642 sub-3 nm particles using a particle size magnifier in different environments: from clean mountain top to polluted
643 megacities, *Atmos. Chem. Phys.*, 17(3), 2163–2187, doi:10.5194/acp-17-2163-2017, 2017.
- 644 Kuang, C., McMurry, P. H., McCormick, A. V. and Eisele, F. L.: Dependence of nucleation rates on sulfuric acid vapor
645 concentration in diverse atmospheric locations, *J. Geophys. Res.*, 113(D10), D10209, doi:10.1029/2007JD009253,
646 2008.
- 647 Kulmala, M. and Kerminen, V. M.: On the formation and growth of atmospheric nanoparticles, *Atmos. Res.*, 90(2–4),
648 132–150, doi:10.1016/j.atmosres.2008.01.005, 2008.
- 649 Kulmala, M., Petäjä, T., Nieminen, T., Sipilä, M., Manninen, H. E., Lehtipalo, K., Dal Maso, M., Aalto, P. P., Junninen,
650 H., Paasonen, P., Riipinen, I., Lehtinen, K. E. J., Laaksonen, A. and Kerminen, V. M.: Measurement of the nucleation
651 of atmospheric aerosol particles, *Nat. Protoc.*, 7(9), 1651–1667, doi:10.1038/nprot.2012.091, 2012.
- 652 Kürten, A., Rondo, L., Ehrhart, S. and Curtius, J.: Calibration of a chemical ionization mass spectrometer for the
653 measurement of gaseous sulfuric acid, *J. Phys. Chem. A*, 116(24), 6375–6386, doi:10.1021/jp212123n, 2012.
- 654 Kuuluvainen, H., Poikkimäki, M., Järvinen, A., Kuula, J., Irjala, M., Dal Maso, M., Keskinen, J., Timonen, H., Niemi,
655 J. V. and Rönkkö, T.: Vertical profiles of lung deposited surface area concentration of particulate matter measured with
656 a drone in a street canyon, *Environ. Pollut.*, 241, 96–105, doi:10.1016/j.envpol.2018.04.100, 2018.
- 657 Lehtipalo, K., Kontkanen, J., Kangasluoma, J., Franchin, A., Wimmer, D., Schobesberger, S., Junninen, H., Petäjä, T.,
658 Sipilä, M., Worsnop, D. R., Kulmala, M., Lehtipalo, K., Mikkilä, J., Vanhanen, J., Leppä, J. and Worsnop, D. R.:
659 Methods for determining particle size distribution and growth rates between 1 and 3 nm using the Particle Size
660 Magnifier, *Boreal Environ. Res.*, 19(September), 215–236, 2014.
- 661 Maher, B. A., Ahmed, I. A. M., Karloukovski, V., MacLaren, D. A., Foulds, P. G., Allsop, D., Mann, D. M. A., Torres-
662 Jardón, R. and Calderon-Garciduenas, L.: Magnetite pollution nanoparticles in the human brain, *Proc. Natl. Acad. Sci.*
663 U. S. A., 113(39), 10797–10801, doi:10.1073/pnas.1605941113, 2016.
- 664 Mårtensson, E. M., Nilsson, E. D., Buzorius, G. and Johansson, C.: Eddy covariance measurements and
665 parameterisation of traffic related particle emissions in an urban environment, *Atmos. Chem. Phys.*, 6(3), 769–785,
666 doi:10.5194/acp-6-769-2006, 2006.
- 667 Mauldin, R. L., Tanner, D. J., Heath, J. A., Huebert, B. J. and Eisele, F. L.: Observations of H₂SO₄ and MSA during



- 668 PEM-Tropics-A, *J. Geophys. Res. Atmos.*, 104(D5), 5801–5816, doi:10.1029/98JD02612@10.1002/(ISSN)2169-
669 8996.PAMTA1, 1999.
- 670 Mylläri, F., Asmi, E., Anttila, T., Saukko, E., Vakkari, V., Pirjola, L., Hillamo, R., Laurila, T., Häyriinen, A.,
671 Rautiainen, J., Lihavainen, H., O'Connor, E., Niemelä, V., Keskinen, J., Dal Maso, M. and Rönkkö, T.: New particle
672 formation in the fresh flue-gas plume from a coal-fired power plant: effect of flue-gas cleaning, *Atmos. Chem. Phys.*,
673 16(11), 7485–7496, doi:10.5194/acp-16-7485-2016, 2016.
- 674 Nieminen, T., Asmi, A., Dal maso, M., Aalto, P. P., Keronen, P., Petäjä, T., Kulmala, M. and Kerminen, V.: Trends in
675 atmospheric new-particle formation: 16 years of observations in a boreal-forest environment. [online] Available from:
676 <http://www.arl>. (Accessed 11 January 2021), 2014.
- 677 Olin, M., Kuuluvainen, H., Aurela, M., Kalliokoski, J., Kuittinen, N., Isotalo, M., Timonen, H. J., Niemi, J. V., Rönkkö,
678 T. and Dal Maso, M.: Traffic-originated nanocluster emission exceeds H₂SO₄-driven photochemical new particle
679 formation in an urban area, *Atmos. Chem. Phys.*, 20(1), 1–13, doi:10.5194/acp-20-1-2020, 2020.
- 680 Pirjola, L., Paasonen, P., Pfeiffer, D., Hussein, T., Hämeri, K., Koskentalo, T., Virtanen, A., Rönkkö, T., Keskinen, J.,
681 Pakkanen, T. A. and Hillamo, R. E.: Dispersion of particles and trace gases nearby a city highway: Mobile laboratory
682 measurements in Finland, *Atmos. Environ.*, 40(5), 867–879, doi:10.1016/j.atmosenv.2005.10.018, 2006.
- 683 Ramanathan, V. and Feng, Y.: Air pollution, greenhouse gases and climate change: Global and regional perspectives,
684 *Atmos. Environ.*, 43(1), 37–50, doi:10.1016/j.atmosenv.2008.09.063, 2009.
- 685 Ripamonti, G., Järvi, L., Mølgaard, B., Hussein, T., Nordbo, A. and Hämeri, K.: The effect of local sources on aerosol
686 particle number size distribution, concentrations and fluxes in Helsinki, Finland, *Tellus, Ser. B Chem. Phys. Meteorol.*,
687 65(1), 19786, doi:10.3402/tellusb.v65i0.19786, 2013.
- 688 Rönkkö, T. and Timonen, H.: Overview of Sources and Characteristics of Nanoparticles in Urban Traffic-Influenced
689 Areas, *J. Alzheimer's Dis.*, 72(1), 15–28, doi:10.3233/JAD-190170, 2019.
- 690 Rönkkö, T., Kuuluvainen, H., Karjalainen, P., Keskinen, J., Hillamo, R., Niemi, J. V., Pirjola, L., Timonen, H. J.,
691 Saarikoski, S., Saukko, E., Järvinen, A., Silvennoinen, H., Rostedt, A., Olin, M., Yli-Ojanperä, J., Nousiainen, P.,
692 Kousa, A. and Dal Maso, M.: Traffic is a major source of atmospheric nanocluster aerosol, *Proc. Natl. Acad. Sci. U. S.*
693 *A.*, 114(29), 7549–7554, doi:10.1073/pnas.1700830114, 2017.
- 694 Rose, C., Zha, Q., Dada, L., Yan, C., Lehtipalo, K., Junninen, H., Mazon, S. B., Jokinen, T., Sarnela, N., Sipilä, M.,
695 Petäjä, T., Kerminen, V. M., Bianchi, F. and Kulmala, M.: Observations of biogenic ion-induced cluster formation in
696 the atmosphere, *Sci. Adv.*, 4(4), 1–11, doi:10.1126/sciadv.aar5218, 2018.
- 697 Rosenfeld, D., Lohmann, U., Raga, G. B., O'Dowd, C. D., Kulmala, M., Fuzzi, S., Reissell, A. and Andreae, M. O.:
698 Flood or drought: How do aerosols affect precipitation?, *Science* (80-.), 321(5894), 1309–1313,
699 doi:10.1126/science.1160606, 2008.
- 700 Salma, I., Borsós, T., Weidinger, T., Aalto, P., Hussein, T., Dal Maso, M. and Kulmala, M.: Production, growth and
701 properties of ultrafine atmospheric aerosol particles in an urban environment, *Atmos. Chem. Phys.*, 11(3), 1339–1353,
702 doi:10.5194/acp-11-1339-2011, 2011.



- 703 Seinfeld, J. H. and Pandis, S. N.: Atmospheric Chemistry and Physics: From Air Pollution to Climate Change., 2016.
- 704 Sipila, M., Berndt, T., Petaja, T., Brus, D., Vanhanen, J., Stratmann, F., Patokoski, J., Mauldin, R. L., Hyvärinen, A. P.,
705 Lihavainen, H. and Kulmala, M.: The role of sulfuric acid in atmospheric nucleation, *Science* (80-.), 327(5970), 1243–
706 1246, doi:10.1126/science.1180315, 2010.
- 707 Tauber, C., Brilke, S., Wlasits, P. J., Bauer, P. S., Köberl, G., Steiner, G. and Winkler, P. M.: Humidity effects on the
708 detection of soluble and insoluble nanoparticles in butanol operated condensation particle counters, *Atmos. Meas.*
709 *Tech.*, 12(7), 3659–3671, doi:10.5194/amt-12-3659-2019, 2019.
- 710 Tian, L., Shang, Y., Chen, R., Bai, R., Chen, C., Inthavong, K. and Tu, J.: Correlation of regional deposition dosage for
711 inhaled nanoparticles in human and rat olfactory, *Part. Fibre Toxicol.*, 16(1), 6, doi:10.1186/s12989-019-0290-8, 2019.
- 712 Vanhanen, J., Mikkilä, J., Lehtipalo, K., Sipilä, M., Manninen, H. E., Siivola, E., Petäjä, T. and Kulmala, M.: Particle
713 Size Magnifier for Nano-CN Detection, *Aerosol Sci. Technol.*, 45(4), 533–542, doi:10.1080/02786826.2010.547889,
714 2011.
- 715 Viggiano, A. A., Seeley, J. V., Mundis, P. L., Williamson, J. S. and Morris, R. A.: Rate Constants for the Reactions of
716 $XO_3 - (H_2O)_n$ ($X = C, HC, \text{ and } N$) and $NO_3 - (HNO_3)_n$ with H_2SO_4 : Implications for Atmospheric
717 Detection of H_2SO_4 , *J. Phys. Chem. A*, 101(44), 8275–8278, doi:10.1021/jp971768h, 1997.
- 718 Wang, Z. B., Hu, M., Yue, D. L., Zheng, J., Zhang, R. Y., Wiedensohler, A., Wu, Z. J., Nieminen, T. and Boy, M.:
719 Evaluation on the role of sulfuric acid in the mechanisms of new particle formation for Beijing case, *Atmos. Chem.*
720 *Phys.*, 11(24), 12663–12671, doi:10.5194/acp-11-12663-2011, 2011.
- 721 Wiedensohler, A., Birmili, W., Nowak, A., Sonntag, A., Weinhold, K., Merkel, M., Wehner, B., Tuch, T., Pfeifer, S.,
722 Fiebig, M., Fjåraa, A. M., Asmi, E., Sellegri, K., Depuy, R., Venzac, H., Villani, P., Laj, P., Aalto, P., Ogren, J. A.,
723 Swietlicki, E., Williams, P., Roldin, P., Quincey, P., Hüglin, C., Fierz-Schmidhauser, R., Gysel, M., Weingartner, E.,
724 Riccobono, F., Santos, S., Gröning, C., Faloon, K., Beddows, D., Harrison, R., Monahan, C., Jennings, S. G.,
725 O'Dowd, C. D., Marinoni, A., Horn, H.-G., Keck, L., Jiang, J., Scheckman, J., McMurry, P. H., Deng, Z.,
726 Zhao, C. S., Moerman, M., Henzing, B., de Leeuw, G., Löschau, G. and Bastian, S.: Mobility particle size
727 spectrometers: harmonization of technical standards and data structure to facilitate high quality long-term observations
728 of atmospheric particle number size distributions, *Atmos. Meas. Tech.*, 5(3), 657–685, doi:10.5194/amt-5-657-2012,
729 2012.
- 730 Williamson, J. H.: Least-squares fitting of a straight line, *Can. J. Phys.*, 46(16), 1845–1847, doi:10.1139/p68-523,
731 1968.
- 732 Winkler, P. M., Steiner, G., Vrtala, A., Vehkamäki, H., Noppel, M., Lehtinen, K. E. J., Reischl, G. P., Wagner, P. E.
733 and Kulmala, M.: Heterogeneous nucleation experiments bridging the scale from molecular ion clusters to
734 nanoparticles, *Science* (80-.), 319(5868), 1374–1377, doi:10.1126/science.1149034, 2008.
- 735 Wlasits, P. J., Stolzenburg, D., Tauber, C., Brilke, S., Schmitt, S. H., Winkler, P. M. and Wimmer, D.: Counting on
736 chemistry: laboratory evaluation of seed-material-dependent detection efficiencies of ultrafine condensation particle
737 counters, *Atmos. Meas. Tech.*, 13(7), 3787–3798, doi:10.5194/amt-13-3787-2020, 2020.



- 738 Wonaschütz, A., Demattio, A., Wagner, R., Burkart, J., Ziková, N., Vodička, P., Ludwig, W., Steiner, G., Schwarz, J.
739 and Hitznerberger, R.: Seasonality of new particle formation in Vienna, Austria - Influence of air mass origin and
740 aerosol chemical composition, *Atmos. Environ.*, 118, 118–126, doi:10.1016/j.atmosenv.2015.07.035, 2015.
- 741 Xiao, S., Wang, M. Y., Yao, L., Kulmala, M., Zhou, B., Yang, X., Chen, J. M., Wang, D. F., Fu, Q. Y., Worsnop, D. R.
742 and Wang, L.: Strong atmospheric new particle formation in winter in urban Shanghai, China, *Atmos. Chem. Phys.*,
743 15(4), 1769–1781, doi:10.5194/acp-15-1769-2015, 2015.
- 744 Yao, L., Garmash, O., Bianchi, F., Zheng, J., Yan, C., Kontkanen, J., Junninen, H., Mazon, S. B., Ehn, M., Paasonen,
745 P., Sipilä, M., Wang, M., Wang, X., Xiao, S., Chen, H., Lu, Y., Zhang, B., Wang, D., Fu, Q., Geng, F., Li, L., Wang,
746 H., Qiao, L., Yang, X., Chen, J., Kerminen, V. M., Petäjä, T., Worsnop, D. R., Kulmala, M. and Wang, L.: Atmospheric
747 new particle formation from sulfuric acid and amines in a Chinese megacity, *Science* (80-.), 361(6399), 278–281,
748 doi:10.1126/science.aao4839, 2018.
- 749 York, D.: Least-squares fitting of a straight line, *Can. J. Phys.*, 44, 1079–1086, 1966.
- 750 Zhou, Y., Dada, L., Liu, Y. Y., Fu, Y., Kangasluoma, J., Chan, T., Yan, C., Chu, B., Daellenbach, K. R., Bianchi, F.,
751 Kokkonen, T. V., Liu, Y. Y., Kujansuu, J., Kerminen, V. M., Petäjä, T., Wang, L., Jiang, J., Kulmala, M., Xiao, S.,
752 Wang, M. Y., Yao, L., Kulmala, M., Zhou, B., Yang, X., Chen, J. M., Wang, D. F., Fu, Q. Y., Worsnop, D. R. and
753 Wang, L.: Variation of size-segregated particle number concentrations in wintertime Beijing, *Atmos. Chem. Phys.*,
754 20(2), 1201–1216, doi:10.5194/acp-20-1201-2020, 2020.
- 755 Zhu, Y., Hinds, W. C., Kim, S. and Sioutas, C.: Concentration and size distribution of ultrafine particles near a major
756 highway, *J. Air Waste Manag. Assoc.*, 52(9), 1032–1042, doi:10.1080/10473289.2002.10470842, 2002.
- 757